NATIONAL ADVISORY COMMITTEE FOR AERONAUTICS

TECHNICAL NOTE 4260

GROUND REFLECTION OF JET NOISE

By Walton L. Howes

Lewis Flight Propulsion Laboratory
Cleveland, Ohio

Washington
April 1958

NATIONAL ADVISORY COMMITTEE FOR AERONAUTICS

TECHNICAL NOTE 4260

GROUND REFLECTION OF JET NOISE

By Walton L. Howes

SUMMARY

The effect of a reflecting plane on the propagation of jet noise was investigated theoretically and experimentally. The study is particularly directed toward determining the free-field spectrum of subsonic-jet noise from measurements made in the presence of a ground plane.

Characteristics of the decay of jet noise in the free field are discussed, and crude estimates of the free-field spectrum of jet noise are made from available experimental data. The theory of far-field noise decay in the presence of specular ground reflections is expanded. By using the decay theory and spectrum estimates, decay characteristics at constant height above a reflecting plane are computed for various values of ground impedance and receiver band-pass width. The effects on decay of spectrum shape and nonideal filtering are studied.

In addition to the decay characteristics noted by Franken, it is shown that the decay of jet noise is practically independent of the spectrum shape, so that the decay can be represented by the decay of a white spectrum. Nonideal filtering may have a slight effect on measured decay curves. The excess decay resulting from the longer path length of the reflected noise over that of the noise received directly from the source has a negligible effect on the decay curve.

By considering the characteristics of the theoretical decay curves, an empirical procedure for correcting measured spectra to obtain corresponding free-field spectra is developed and tested.

Jet-noise measurements along a radius in a plane 10 feet above a grassy surface indicated that reflection effects were experimentally significant and could be evaluated quantitatively. Spectra corrected according to the proposed procedure satisfied the theoretical prediction that the free-field spectrum shape be independent of the distance from the source when measured in the far field. Other characteristics of the spectra and decay curves were found to be in agreement with theory, at least qualitatively. The onset of the acoustic far field was found to occur at a distance of 10 wavelengths from the source at an azimuth of 30° or 330° with respect to the jet axis.

INTRODUCTION

The study of jet noise and methods for suppressing noise produced by various jet propulsion devices requires that the noise fields be measured. Measurements of the noise in operational situations, as from flybys of jet aircraft, are useful for noise-nuisance studies but are not very useful for studying the relation between jet flow and jet noise. For studies of the latter type stricter control of experimental conditions is required.

In relating the noise to the flow, the free-space, or free-field, spectrum of jet noise is ultimately the quantity of interest. In tests made outdoors, repeatable noise measurements can be performed by using stationary jet nozzles in a relatively quiescent isothermal atmosphere. However, the immediate presence of ground introduces a disturbing factor which prevents direct determination of the free-space noise field (ref. 1). Reflection of noise from the ground can be associated with apparent noise sources of appreciable strength. These sources are images of the jet-noise source. At an acoustic receiver the reflected noise is coherent, or correlated, with the noise received directly from the jet so that interference between the direct and reflected noise occurs.

The present investigation resulted from an attempt to explain certain unexpected anomalies which appeared in jet-noise data reported in reference 2. These anomalies consisted of unexpected peaks and valleys in otherwise smooth spectra and were presumably caused by reflections.

ANALYSIS

The following analysis is concerned with the problem of measuring noise when the source and receiver are located above a reflecting plane. The noise spectrum is assumed to be continuous, and the receiver bandpass width is selected arbitrarily. Relations will be established between the free-field noise spectrum (reflecting plane absent) and the corresponding spectrum obtained with the reflecting surface present. The spectra of primary interest herein are the

(1) mean-square-pressure spectrum, $\overline{p^2(f)}$

(2) sound-pressure-level spectrum, $SPL(f_a,f_b) = 10 \log \left[\overline{p^2(f_a,f_b)}/p_o'^2 \right]$

where p is acoustic pressure, f is frequency, f_a and f_b are lower and upper cutoff frequencies, respectively, associated with an acoustic receiver, and p_o' is a reference pressure (2×10^{-4} dynes/cm^2). The horizontal bar denotes a time average. (All symbols are defined in appendix A.)

The cutoff frequencies f_a and f_b imply a sharp cutoff of the receiver pass band in the filtering process, an ideal, but unattainable, condition. However, in the present report ideal filtering generally will be assumed.

Free Field

Before the effects of ground reflections are considered, the free-field conditions will be defined. The free field consists of a quiescent isothermal atmosphere free of reflecting surfaces and atmospheric attenuation. Also, in the subsequent analysis, it will be assumed that

(1) The noise source is statistically stationary, that is, the statistical properties of the noise are unchanged when measured at different times.

(2) The measurements are performed in the acoustic far field, namely, at a distance from the source which is large compared to the acoustic wavelength.

Because a jet is presumed to contain a multitude of multipole noise sources (refs. 3 and 4), which collectively comprise an extended source, it will also be assumed that

(3) The measurements are performed at a distance from the source which is large compared to the size of the extended source.

For the preceding conditions the decay of acoustic pressure as a function of distance from the noise source obeys the well-known inverse-square law of decay, namely,

$$\overline{p^2(f)} \propto 1/r^2 \tag{1}$$

Thus, in the far field the shapes of the noise spectra at points along a radius having its origin at the noise source are independent of the distance from the source. This is in contrast to the situation in the near field, that is, at distances from the source which are not large compared to the acoustic wavelength. In the near field the spectrum shape is dependent on the distance from the source because the decay rate is frequency dependent. For example, in a subsonic jet the predominant sources are presumed to be quadrupoles (refs. 3 and 4). For a single quadrupole source the root-mean-square pressure at a distance r from the source can be shown to have the form

$$\sqrt{\overline{p^2(f)}} = q(f)\left(\frac{\varphi_1}{r} + \frac{\varphi_2}{fr^2} + \frac{\varphi_3}{f^2r^3}\right) \tag{2}$$

where $q(f)$ relates essentially to the source strength, and the φ's are essentially directional functions. Equation (2) satisfies the inverse-square decay law for the far field and illustrates the frequency dependence of the decay rate in the near field.

Free-Field Spectrum

The noise spectrum with reflections is a function of the free-field spectrum. Therefore, in order to predict the effect of reflections, the free-field spectrum must first be estimated.

The jet-engine-noise spectra presented in figures 13(a) to (d) of reference 5 and replotted herein in figure 1 approximate free-field spectra in that the direct acoustic path length from the source to the receiver was considerably less than (<1/3) the reflection path via the ground. However, these spectra are near-field spectra obtained very close to the engine exhaust.

According to equation (2), the far-field spectrum $\overline{[p^2(f)]_F}$ resulting from a single quadrupole source is related to the near-field spectrum $\overline{[p^2(f)]_N}$ by

$$\overline{[p^2(f)]_F} \approx \left(\frac{\varphi_1}{\varphi_3}\right)^2 \frac{r_N^6}{r_F^2} f^4 \overline{[p^2(f)]_N} \tag{3}$$

which indicates that, compared with the near-field spectrum, the far-field spectrum is weighted heavily toward higher frequencies. In reality, the weighting would be damped significantly at high frequencies by atmospheric attenuation (ref. 6).

Although the engine-noise spectra, as well as the air-jet data, which are presented in the section entitled EXPERIMENT, were obtained for nozzle pressure ratios slightly greater than for choking, it is believed that deformation of the spectrum at these pressure ratios by discrete acoustic frequencies caused by shocks is small or negligible (refs. 7 and 5).

In general, in the free field the near- and far-field spectra shapes should not differ greatly although the noise levels and the frequency of the spectra peaks may differ considerably. The engine-noise spectra possess a shape similar to those for subsonic-jet noise in a reverberant chamber (ref. 8) and the theoretical noise intensity from isotropic turbulence (ref. 9). Thus, the shapes of the spectra in figure 1 will be regarded as representative of the shapes of free-field spectra of jet noise for constant-percentage band width.

The sound-pressure-level spectra are plotted in figure 1 as a function of a dimensionless frequency ratio $m^* = m/\mu$, where μ is the frequency of the peak of the corresponding spectral density curve ((mean-square pressure)/cps). The spectra in figure 1 are replotted in figure 2 in the form of a spectral density ratio $[\overline{p^2(f^*)}]/[\overline{p^2(f^* = 1)}]$ as a function of the frequency ratio f^* by using the relations

$$\frac{\overline{p^2(f)}}{p_o^2} \approx \text{antilog}\left[\frac{SPL(f_a,f_b)}{10} - \log(f_b - f_a)\right]$$

$$\frac{\overline{p^2(f^*)}}{\overline{p^2(f^* = 1)}} = \frac{\overline{p^2(f)}}{p_o^2} \frac{p_o^2}{\overline{p^2(\mu)}}$$

where p_o is the reference pressure (2×10^{-4} dyne-sec/cm^2) and $\overline{p^2(\mu)}$ is the maximum spectral density. In the spectral density form the spectrum formulations are directly applicable in the subsequent analysis.

Simple dimensionless closed expressions which resemble the experimental density spectra include the Gaussian expression

$$\frac{\overline{p^2(f^*)}}{\overline{p^2(f^* = 1)}} = e^{-u^2} \tag{4}$$

where

$$u = \frac{f^* - 1}{\sigma^*}$$

$$\sigma^* = \frac{\sigma}{\mu}$$

and the expression

$$\frac{\overline{p^2(f^*)}}{\overline{p^2(f^* = 1)}} = f^* e^{1-f^*} \tag{5}$$

The dimensionless density spectra defined by equations (4) and (5) are included in figure 2 for comparison with experimental results. Equations for the corresponding SPL spectra for arbitrary band width are derived in appendix B. The resulting SPL spectra for 1/3-octave band

widths are shown in figure 1 for comparison with the experimental data. Although these spectra fit the experimental data rather poorly, they will nevertheless prove useful in determining the effect of a change of spectrum shape on decay characteristics.

Ground Reflection (Theoretical Analysis)

If a reflecting plane such as ground is introduced, the original free-field noise distribution and, therefore, the recorded noise spectra will be modified by interference between direct and reflected noise. The decay of noise as a function of distance has previously been analyzed theoretically in reference 1. This analysis is restricted to the cases of a band-limited white spectrum or a pure-tone receiver (arbitrary spectrum).

Consequently, in the following analysis decay curves are computed for a few spectrum functions in addition to the band-limited white spectrum in order to find the significance of spectrum shape with respect to decay fluctuations. The spectrum shapes and constants have been selected to conform to the estimates presented in the section Free-Field Spectrum. The effect of nonideal filtering of the received signal is studied.

Consider a jet-noise source and acoustic receiver located above a ground plane (fig. 3). Surface irregularities will be regarded as small compared to the acoustic wavelength so that the reflection is specular. The initial assumptions will be the same as those listed in the section Free Field.

First, the case of an arbitrary spectrum and a pure-tone (f_o) receiver will be considered. The procedure in reference 1 is adopted.

Let P represent the resultant pressure at the receiver and p represent the direct or reflected component pressures; let Q represent the impedance of the reflecting plane. The mean-square pressure at the receiver is given by

$$\overline{P^2(f_o)} = \overline{p^2(f_o)}$$

when the reflector is absent, and

$$\overline{p^2(f_o,\tau)} = \overline{\left[p(f_o) + Q(f_o)p(f_o,\tau)\right]^2}$$

$$= \overline{p^2(f_o)} + Q^2(f_o)\overline{p^2(f_o,\tau)} + 2\psi(f_o,\tau)$$

when the reflector is present; Ψ is the autocorrelation function given by

$$\Psi(f_o,\tau) = Q(f_o)\overline{p(f_o)p(f_o,\tau)}$$

$$= \mathscr{R}(f_o,\tau)\sqrt{Q^2(f_o)\overline{p^2(f_o)}\ \overline{p^2(f_o,\tau)}} \tag{7}$$

where $\mathscr{R}$ is the autocorrelation coefficient. The pressures $p(f_o)$ and $Q(f_o)p(f_o,\tau)$ are received simultaneously. The pressure $p(f_o)$ arrives directly from the source, whereas $p(f_o,\tau)$ is emitted τ seconds earlier than $p(f_o)$ and arrives at the receiver via the longer reflected path.

The ratio of the mean-square pressure with reflection to the free-field mean-square pressure is

$$R(f_o,\tau) = \frac{\overline{P^2(f_o,\tau)}}{\overline{P^2(f_o)}} = 1 + Q^2(f_o)\frac{\overline{p^2(f_o,\tau)}}{\overline{p^2(f_o)}} + 2Q(f_o)\left[\frac{\overline{p^2(f_o,\tau)}}{\overline{p^2(f_o)}}\right]^{1/2}\frac{\Psi(f_o,\tau)}{\sqrt{Q^2(f_o)\overline{p^2(f_o)}\ \overline{p^2(f_o,\tau)}}}$$

In the far field, by virtue of the inverse-square law of decay,

$$\overline{p^2(f_o,\tau)}/\overline{p^2(f_o)} = (r/r_R)^2 \tag{8}$$

where r_R is the acoustic path length via the reflector (fig. 3). Therefore, substituting from equations (7) and (8) into the equation for $R(f_o,\tau)$ gives

$$R(f_o,\tau) = 1 + (r/r_R)^2Q^2(f_o) + 2(r/r_R)Q(f_o)\mathscr{R}(f_o,\tau) \tag{9}$$

for a pure-tone receiver.

By considering figure 3,

$$\left(\frac{r}{r_R}\right)^2 = \frac{x^2 + (H - h)^2}{x^2 + (H + h)^2} \tag{10}$$

and

$$\tau = \frac{r_R}{a}\left(1 - \frac{r}{r_R}\right) \tag{11}$$

If, now, the pure-tone receiver is replaced by a receiver having a finite band width $f_b - f_a$, the terms $p^2(f)$ and product terms $Q^2(f)p^2(f,\tau)$ must be integrated separately with respect to f throughout the interval f_a, f_b. Integration of the $Q^2\overline{p^2}$ terms becomes exceedingly difficult for all except the simplest spectra. However, to illustrate the general result, let

$$\overline{p^2(Q,f_a,f_b,\tau)} = \int_{f_a}^{f_b} Q^2(f)\overline{p^2(f,\tau)}\,df$$

Then, the band-pass equivalent of equation (9) becomes

$$R(f_a,f_b,\tau) = \frac{\overline{p^2(f_a,f_b,\tau)}}{\overline{p^2(f_a,f_b)}}$$

$$= 1 + \frac{\overline{p^2(Q,f_a,f_b,\tau)}}{\overline{p^2(f_a,f_b)}} + 2\left[\frac{\overline{p^2(Q,f_a,f_b,\tau)}}{\overline{p^2(f_a,f_b)}}\right]^{1/2} \mathscr{R}(f_a,f_b,\tau) \qquad (12)$$

If the band-pass width is unlimited,

$$R(\tau) = 1 + \frac{\overline{p^2(Q,\tau)}}{\overline{p^2}} + 2\left[\frac{\overline{p^2(Q,\tau)}}{\overline{p^2}}\right]^{1/2} \mathscr{R}(\tau) \qquad (12a)$$

In addition to being defined for arbitrary band width by

$$\mathscr{R}(f_a,f_b,\tau) = \frac{\overline{p(f_a,f_b)p(f_a,f_b,\tau)}}{\sqrt{\overline{p^2(f_a,f_b)}\;\overline{p^2(f_a,f_b,\tau)}}} \qquad (13)$$

$\mathscr{R}(f_a,f_b,\tau)$ is also the Fourier transform of the spectrum; that is, from reference 10,

$$\mathscr{R}(f_a,f_b,\tau) = \mathscr{R}_e \frac{1}{\overline{p^2(f_a,f_b)}} \int_{f_a}^{f_b} \overline{p^2(f)}e^{2\pi i f\tau}\,df \qquad (14)$$

For an assumed spectrum $\overline{p^2(f)}$, the correlation coefficient $\mathscr{R}$ may be computed from equation (14) (ref. 11). If the functional dependence of Q is assumed, the acoustic pressure ratio R may be computed in certain instances from equation (12) by utilizing equations (10) and (11). Decay curves can be determined as a function of the horizontal separation x of the source and receiver by performing the preceding computations and then including the additional effect of inverse-square-law decay utilizing the relation

$$\dot{SPL} = 10 \log \frac{R}{x^2} \tag{15}$$

Solutions for the autocorrelation coefficient $\mathscr{R}$ for various spectra and receiver band widths are derived in appendix C. The associated formulas for the acoustic pressure ratio R are as follows:

(1) Pure-tone receiver:

(a) Perfect reflector, arbitrary spectrum:

$$R(f_o,\tau) = 1 + (r/r_R)^2 + 2(r/r_R)\cos 2\pi f_o \tau \tag{16}$$

(b) Imperfect reflector, arbitrary spectrum:

$$R(f_o,\tau) = 1 + (r/r_R)^2 Q^2(f_o) + 2(r/r_R)Q(f_o)\cos 2\pi f_o \tau \tag{17}$$

(2) Gaussian spectrum:

(a) Unlimited band width, perfect reflector:

$$R(\tau) = 1 + (r/r_R)^2 + 2(r/r_R)e^{-\gamma^2}\cos\alpha \tag{18}$$

where $\alpha = 2\pi\mu\tau$ and $\gamma = \pi\sigma\tau$.

(b) Limited band width, perfect reflector:

$$R(f_a,f_b,\tau) = 1 + \left(\frac{r}{r_R}\right)^2 + 2\frac{r}{r_R}\mathscr{R}e\left[e^{-\gamma^2}e^{i\alpha}\frac{\operatorname{erf}(u_b - i\gamma) - \operatorname{erf}(u_a - i\gamma)}{\operatorname{erf} u_b - \operatorname{erf} u_a}\right] \tag{19}$$

where $u_a = (f_a - \mu)/\sigma$ and $u_b = (f_b - \mu)/\sigma$.

(3) $f^*e^{1-f^*}$ Spectrum:

(a) Unlimited band width, perfect reflector:

$$R(\tau) = 1 + \left(\frac{r}{r_R}\right)^2 + 2\,\frac{r}{r_R}\,\frac{1 - \alpha^2}{(1 + \alpha^2)^2} \tag{20}$$

(b) Limited band width, perfect reflector:

$$R(f_a,f_b,\tau) = 1 + (r/r_R)^2 + 2(r/r_R)$$
$$\left[(1 + \alpha^2)^2\left(z_b e^{-f_b/\mu} - z_a e^{-f_a/\mu}\right)\right]^{-1}$$
$$\left[(1 - \alpha^2)\left(z_b e^{-f_b/\mu}\cos y_b - z_a e^{-f_a/\mu}\cos y_a + y_b e^{-f_b/\mu}\sin y_b - y_a e^{-f_a/\mu}\sin y_a\right) - 2\alpha\left(z_b e^{-f_b/\mu}\sin y_b - z_a e^{-f_a/\mu}\sin y_a - y_b e^{-f_b/\mu}\cos y_b + y_a e^{-f_a/\mu}\cos y_a\right)\right] \tag{21}$$

where $z_a = (f_a/\mu) + 1$, $z_b = (f_b/\mu) + 1$, $y_a = 2\pi f_a\tau$, and $y_b = 2\pi f_b\tau$.

(4) White spectrum:

(a) Unlimited band width, perfect reflector:

$$R(\tau) = 1 + (r/r_R)^2 \tag{22}$$

(b) Limited band width, perfect reflector:

$$R(f_a,f_b,\tau) = 1 + \left(\frac{r}{r_R}\right)^2 + 2\,\frac{r}{r_R}\left\{\frac{\sin\left[\pi(f_b - f_a)\tau\right]}{\pi(f_b - f_a)\tau}\cos\left[\pi(f_b + f_a)\tau\right]\right\} \tag{23}$$

$$R(f_a,f_b,0) = 4$$

(c) Limited band width, arbitrary ground impedance constant within band:

$$R(f_a,f_b,\tau) = 1 + Q^2(f_a,f_b)\left(\frac{r}{r_R}\right)^2 + 2Q(f_a,f_b)\,\frac{r}{r_R}\left\{\frac{\sin\left[\pi(f_b - f_a)\tau\right]}{\pi(f_b - f_a)\tau}\cos\left[\pi(f_b + f_a)\tau\right]\right\} \quad (24)$$

where, for plane waves (ref. 12),

$$Q(f_a,f_b) \approx \frac{\frac{h + H}{x} - \beta}{\frac{h + H}{x} + \beta}$$

(d) Nonideal filter (Gaussian transfer function), perfect reflector:

$$R(\tau) = 1 + (r/r_R)^2 + 2(r/r_R)e^{-\gamma'^2}\cos\alpha' \quad (25)$$

where $\alpha' = 2\pi m\tau$ and $\gamma' = \pi\rho\tau$.

Decay Characteristics

In reference 1 space fluctuations of mean-square pressure as a function of receiver distance and at fixed height above the plane were predicted. Decreasing the filter mean frequency or band width or the height of the source or receiver was shown to intensify the fluctuations. Varying the plane impedance shifted the locations of the fluctuation maximums and minimums.

Additional characteristics of acoustic decay as a function of the source-receiver separation at a constant height above the reflecting plane are indicated by the preceding specific solutions for the acoustic mean-square-pressure ratio R. The usual limiting cases

$$R(f_o,\tau) \to 2 + 2\cos 2\pi f_o\tau \qquad \text{(pure-tone receiver)}$$

as $f_b - f_a \to 0$ and

$$R \to 4 \qquad \text{(infinite source-receiver separation)}$$

as $\tau \to 0$ (except possibly for a white unlimited spectrum) result if the reflector is perfect and $h, H \ll x$. As $x \to \infty$ the free-field decay rate (inverse-square law) is approached. The average value of R increases as x is increased. This is not unexpected because $R \to 1$ near

the source, whereas $R \to 4$ as $x \to \infty$. Superimposed on the average increase of R with increasing x is a fluctuation which results from interference of the direct and reflected noise.

Effect of reflected noise on average decay rate. - The condition $\tau \to 0$ corresponds to the situation where $x \to \infty$. If a less stringent height-distance relation is imposed, then from second-order approximations of equations (10) and (11)

$$r/r_R \approx 1 - (2hH/x^2)$$

$$\tau \approx 2hH/(ax)$$

so that

$$R \approx \left[2 - (4hH/x^2)\right] \quad (1 + \mathscr{R})$$

The presence of the term $-4hH/x^2$ indicates that the reflecting plane causes the average decay rate to be somewhat less than the free-field decay rate (inverse-square law). The exact effect of this modified decay law, which results from the excess acoustical path length of the reflected noise, is shown in figure 4 for a pure-tone receiver and perfect reflector. The effect is most apparent at the maximums of the decay fluctuations but is negligible at all values of x.

Decay of fluctuation maximums. - Knowledge of the decay of the fluctuation maximums will prove useful in correcting measured spectra for ground reflections. The extreme values of the decay fluctuations occur where

$$f_o\tau = n \begin{cases} \text{maximums when } n = 0,1,2, \ldots \\ \text{minimums when } n = 1/2,\ 3/2,\ 5/2, \ldots \end{cases}$$

for a pure-tone receiver and perfect reflector. The maximum associated with $n = 0$ corresponds to the condition $\tau = 0$. Geometrically, $\tau \approx 2hH/(ax)$, so that the locations of the interference extremes occur at discrete values x_n given by

$$x_n \approx 2hHf_o/(na)$$

where $n = 0$ corresponds to $x \to \infty$. The preceding approximation for x_n is satisfactory only for small values of n. For n small the decay of the fluctuation maximums essentially obeys the inverse-square law (cf., fig. 4). Therefore, the maximums fall roughly along a straight line if the decay curve is plotted on a log-log scale, for instance, SPL as a function of log x. The result is similar if the reflecting plane has arbitrary impedance (fig. 5).

Loci of fluctuation maximums and minimums. - It is noteworthy that the loci of maximums and minimums are functions of the ground impedance (fig. 5). Seemingly, the determination of these loci could serve as a practical method for determining ground impedance at a particular frequency. Unfortunately, the loci also are functions of the receiver band width as shown in figure 6, which illustrates decay curves for the spectrum $f^*e^{1-f^*}$. An excessive number of calculations is, therefore, required in order to locate maximums and minimums for the general case of arbitrary ground impedance and band width.

In addition to the band-width effect, the frequency influences the possibility of locating maximums and minimums. With increasing frequency the spacing between maximums and minimums is compressed. For high frequencies this spacing may easily be of the same order of magnitude as the spacewise resolution of measurements.

Spectrum shape. - The decay curve obtained using a pure-tone receiver is, of course, independent of the noise spectrum. However, the corresponding result to be expected using a band-pass receiver is not obvious. Thus, the two assumed representations of the jet-noise spectrum (eqs. (4) and (5)) have been applied to determine the effect of spectrum shape on decay for finite and infinite pass bands. The resulting decay curves are shown in figures 7 and 8. In addition, the simpler white spectrum result is also shown. Finally, including the free-field decay curve illustrates the over-all acoustic pressure rise resulting from the influence of the ground.

The decay curves for an infinite pass band are shown in figure 7. The disagreement between the three curves is everywhere less than 2.5 decibels. Decay curves for three 1/3-octave bands are presented in figure 8. The spectrum peak frequency was adopted as the midfrequency of one band. Bands having midfrequencies less than and greater than the peak frequency constitute the other two cases. The 1/3-octave pass-band decay curves differ everywhere by less than 1 decibel, except for the Gaussian curve for the highest frequency band (midfrequency, 1250 cps) where the difference is as great as 5 decibels. From the standpoint of jet-noise measurements the preceding differences are generally insignificant except possibly for high frequencies. The spectrum shape generally appears to have only a minor effect on the decay curve. Thus, the decay curves for the white spectrum should adequately represent the decay of jet noise.

Nonideal filtering. - From the preceding result it might be deduced that, because spectrum shape has only a minor influence on decay, nonideal filtering, which amounts to changing the shape of the filter curve, should also have little effect on the decay curve. However, the over-all

band width of a nonideal filter may differ considerably from that of its ideal counterpart. Because band width is a major factor in determining the decay curve, the preceding deduction may be invalid.

The case of a white spectrum input to a nonideal filter having a Gaussian transfer characteristic (eq. (25)) has been included in the list of acoustic pressure ratio solutions. The Gaussian transfer function yields a decay curve corresponding to that for an unfiltered Gaussian spectrum. However, with nonideal filtering the decay constants are determined by the filter, whereas in the unfiltered case the constants are determined by the spectrum. The values of these constants affect the decay curve.

The decay of a white spectrum obtained with ideal filtering is compared in figure 9 with that which would result from nonideal filtering. A Gaussian transfer function was assumed in the latter case. The total power transferred by the two filters was assumed equal, so that

$$f_b - f_a \approx \sqrt{\pi}\rho \qquad (m > \rho)$$

could be used to compute ρ and, thus, to determine the appropriate transfer function.

The curves in figure 9 show that the filter transfer function may have a slight influence on the measured decay curve. Nonideal filtering tends to dampen the decay fluctuations.

The Gaussian transfer function is not truly representative of the transfer function for a real filter. For a real filter the pass-band limits are finite. Moreover, for a real 1/3-octave filter the transfer function is more nearly a Gaussian function of log f, rather than f. Therefore, the difference of the decay curves in figure 9 is probably extreme.

Reflection Correction

Before attempting to develop a correction procedure for data obtained in the presence of a reflecting plane, methods of eliminating the problem should be considered.

The most obvious method for ameliorating the reflection effects consists of maximizing the source and receiver heights and the analyzer band width. Maximizing the source and receiver heights involves approximating free-field conditions. Practical limitations are likely to restrict this possibility. Maximizing the analyzer band width is undesirable when details of the spectrum are of interest. Possibly the most

desirable solution is to select a perfect reflecting surface. Appropriate values of R, hence the proper corrections, should then be quantitatively predictable from the theory. Experimental evidence is, of course, required to confirm this possibility.

In the following empirical method for determining the free-field noise spectrum, the initial conditions are assumed to be the same as for the preceding theoretical analysis. In addition, the ground impedance is assumed to be independent of frequency and constant between decay peaks. In the proposed procedure the first three steps essentially provide correction for the space fluctuations of SPL resulting from interference between the direct and reflected noise. The final steps provide an over-all combined correction for the effect of ground impedance and the ratio of the peak SPL to the free-field SPL.

The suggested procedure for determining the free-field spectrum associated with a point in the horizontal plane containing the center of the noise source is as follows:

(1) From measured SPL spectra (fig. 10(a)), obtained at several points along a radius through the center of the noise source, plot the measured SPL values for each frequency band as a function of log x (fig. 10(b)).

(2) On each graph construct a line tangent to the predominant SPL peaks (fig. 10(b)). Determine a reflection correction associated with the distance x_o at which the free-field spectrum is desired. This correction is determined for each frequency band and consists of the SPL indicated by the tangent line at the abscissa value x_o minus the SPL indicated by the measured decay curve at the same abscissa value (fig. 10(b)).

(3) Add the appropriate correction to the measured SPL for each frequency band. The resulting corrected spectrum (fig. 10(c)) possesses the shape but not the correct over-all level of the free-field spectrum.

(4) Note the measured over-all SPL associated with the distance x_o, or compute it from the measured spectrum by adding up the power contributions in each frequency band. Similarly, compute the over-all SPL corresponding to the corrected spectrum obtained from step (3).

(5) Compute the difference (corrected over-all SPL minus measured over-all SPL), add 1.5 decibels, and subtract this total from the corrected over-all SPL and from the corrected spectrum. The results obtained correspond to the free-field over-all SPL and the SPL spectrum.

At the end of step (3) the theoretical maximum error resulting from the assumption that the ground impedance is independent of frequency is approximately ±3 decibels for a pure-tone receiver. This value was estimated by taking the level differences of the tangent lines connecting the decay peaks in figure 5 for the various values of β. For a band-pass receiver the maximum error would be less. Moreover, if the true variation of impedance as a function of frequency is continuous, the resulting effect on the corrected spectrum would only amount to a slight distortion of the spectrum shape.

The measured over-all SPL above a perfect reflector is, on the average, approximately 3 decibels higher than the corresponding free-field value (fig. 7). For a surface having arbitrary impedance the difference will be less. For a perfect absorber the difference would be zero. In step (5) a difference of 1.5 decibels is adopted as a reasonable value for a surface having an arbitrary unknown impedance value. The maximum error of the computed free-field spectrum resulting from step (5) would generally be ±1.5 decibels.

The proposed procedure requires a considerable number of additional noise measurements but does not necessitate direct impedance measurements. A single set of data for a given facility is likely to be applicable for all subsequent tests.

The proposed procedure is particularly suited to magnetic-tape recording of data and continuous motion of the microphone whereby continuous decay curves (fig. 10(b)) for all frequencies may be obtained from one microphone traverse.

In the rest of the report, the proposed procedure is tested using experimental data.

EXPERIMENT

Apparatus and Procedure

The noise source consisted of an unheated-air jet issuing from a circular, 4-inch-diameter, convergent nozzle. The jet axis was alined horizontally 10 feet above the ground plane, which was a mowed grassy surface. A schematic diagram and photograph of the facility are shown in figure 11. The nearest large reflecting surfaces, other than the ground, were the walls of two buildings; one about 125 feet upstream, the other approximately 250 feet downstream of the nozzle exit. Reflections from these surfaces were disregarded. The buildings tended to shield the facility from steady winds.

The nozzle pressure ratio was restricted to the constant value 1.99 with variations, resulting mainly from variations of atmospheric conditions, less than 0.01. The nozzle temperature ratio was 1.02. If the results presented in reference 5 are considered, the noise source could be regarded as essentially cylindrical, approximately 4 inches in diameter and $3\frac{1}{2}$ feet long.

Over-all sound-pressure levels were detected using a condenser microphone and were recorded by means of a 1/3-octave band audiofrequency spectrometer-recorder. All sound levels were within the range of linear microphone response. The useful frequency range of the entire system was 35 to 15,000 cycles per second. The microphone response was flat within 1 decibel up to 8,000 cycles per second.

A series of decay measurements were performed at constant microphone height (10 ft) and azimuth (30° and 330° with respect to the jet axis) with variable radial distance. The radial distance was varied in 5-foot increments, and the noise spectrum was recorded at each position. A diagram of the configuration is shown in figure 12. The microphone was mounted on a pole and pointed upward.

Tests were restricted to days when the wind velocity was minimum. In order to account for possible effects of gross atmospheric changes, wind velocity and ambient temperature data were obtained from the United States Weather Bureau station nearby. The values of other atmospheric quantities affecting noise propagation were not determined.

Results

The experimental tests were intended to answer three questions:

(1) Are the ground reflection effects experimentally significant?

(2) Can the reflection effects be disassociated from atmospheric disturbance effects?

(3) Can the reflection effects be evaluated quantitatively?

Typical experimental decay data are shown in figures 13 and 14. The decay of over-all sound-pressure level as a function of distance from the jet nozzle exit is shown in figure 13. From the scatter of these data it is concluded that the repeatability of the acoustic instrumentation was probably within ±1 decibel. Representative decay curves for 1/3-octave band widths are presented in figure 14. The data for run 65 were weighted most heavily in constructing the decay curves because of the completeness and the uniformity of these data and because of the relatively good weather conditions which prevailed during the run.

Obtaining acoustic data over the complete range of available distances necessitated measurements on several different days. The wind direction varied for each run. One set of data (run 64), obtained on a relatively windy day, was measured on the opposite side of the jet from the bulk of the data. Thus, repeatability of the results could be tested. Simultaneous effects of wind and ground roughness and impedance differences, if any, could be observed.

For the 1/3-octave results the predicted space fluctuations characteristic of the reflection effect are generally evident. Peak-to-valley fluctuations were as great as 10 decibels, especially in the interval from 100 to 1000 cycles per second. Thus, the interference effect is significant for measurements in 1/3-octave bands. For all frequency bands having midfrequencies greater than 2000 cycles per second the fluctuations were barely discernible. The disappearance of fluctuations for midfrequencies greater than 2000 cycles per second probably results partially from the fact that the wavelength ($\approx$ 6 in.) approaches the order of magnitude of the ground roughness. The reflection then becomes diffuse, rather than specular, so that the theory discussed in the section entitled Ground Reflection (Theoretical Analysis) no longer applies. Second, atmospheric turbulence and ground roughness likely obscure the closely spaced maximums and minimums by virtue of scattering. Finally, for midfrequencies of the order of 2000 cycles per second and above, the separation of maximums and minimums is of the same order of magnitude as the separation of the measurement points. Thus, the space resolution of the measurements is insufficient to show the loci of maximums and minimums.

In figure 14, the scatter of the data from test run 64 was greater than that from the other tests. However, the reflection effect is still readily apparent. Moreover, the magnitude of the effect is similar to that from the other tests, so that the following conclusions can be drawn:

(1) The wind speed (<12 mph) was not great enough to obscure the reflection effect.

(2) The effect of ground roughness and impedance differences on opposite sides of the jet was generally insignificant. Therefore, the space fluctuations of sound-pressure level could be evaluated quantitatively.

GENERAL RESULTS AND DISCUSSION

The experimental decay rate of over-all SPL (fig. 13) was 20 decibels per distance decade, as predicted by theory, at distances greater than 20 feet from the nozzle exit.

As proposed in the spectrum correction procedure, the average rate of decay for each 1/3 octave was approximated by constructing straight lines tangent to the prominent sound-pressure-level peaks. The indicated average decay rates in decibels per distance decade as a function of mid-frequency are shown in figure 15. The actual decay rates differ markedly from the theoretical rate (inverse-square law) for midfrequencies less than 630 cycles per second. The increased decay rate at the lower frequencies is to be expected if these data are associated with the near field. However, at the lowest frequencies the decay rate is decreased. This effect might possibly result from the fact that the source of low-frequency noise is extended considerably and that the radius is centered at the nozzle exit rather than at the center of the extended source.

The problem is now to find at what distance the far field is attained. The far field is defined loosely as that region where the source-to-observer distance is large compared to the acoustic wavelength. For a single noise source having an arbitrary order of complexity, the onset and continuance of a decay rate of 20 decibels per distance decade (inverse-square law) indicate the beginning of the acoustic far field. The preceding analysis and tests show that the decay curves for narrow band widths are not useful for determining the onset of the far field because of pronounced decay fluctuations resulting from ground reflections. However, the over-all sound-pressure-level decay curve (fig. 13) is relatively free of oscillations because of the extended band width which is involved. For example, the curve in figure 13 attains a slope of 20 decibels per distance decade at a distance approximately 20 feet from the nozzle exit. The sound-pressure-level spectrum at 20 feet is shown in figure 16. The spectrum is relatively symmetrical and peaks at approximately 630 cycles per second. Since pressures associated with frequencies near 630 cycles per second provide the predominant contribution to the over-all sound-pressure level, it follows that for a frequency of 630 cycles per second the acoustic far field is attained at a distance of approximately 10 wavelengths (20 ft) from the source. (Measuring distances from the nozzle, rather than the source, has a negligible effect on this result.)

According to equation (2), the acoustic far field is attained when

$$r \gg \frac{\varphi_2}{\varphi_1} \frac{\lambda}{a}$$

that is, when the first term of equation (2) becomes large compared with the other terms. From the previous estimate the far field is attained when

$$r > \text{const.} \frac{\varphi_2}{\varphi_1} \frac{\lambda}{a} \approx 10\lambda \tag{26}$$

at an azimuth of 30° or 330°. Thus, the distance at which the far field is attained is directly proportional to the acoustic wavelength λ for a fixed azimuth. From the above relation, the onset of the far field can easily be estimated for any frequency. The result, in graphical form, is shown in figure 17. Atmospheric attenuation effects do not appear to be significant for the frequencies and distances involved.

Experimentally obtained sound-pressure-level spectra are shown in figure 18. For each successive spectrum the distance x has been doubled. In each spectrum there is at least one noticeable depression, the frequency of which doubles for each doubling of x. This effect appears to be a reflection effect. These spectra, when corrected for reflection according to the proposed procedure, appear as shown in figure 19. As a result of step (3) of the procedure for determining the free-field spectrum (in the section entitled Ground Reflection), the maximum correction decreased from +10.5 decibels for $x = 25$ feet to +4 decibels for $x = 200$ feet.

The corrected sound-pressure-level spectra have been replotted in figure 20, but the spectra have been readjusted to remove the effect of over-all decay by superimposing the data for the midfrequency of 10,000 cycles per second. For midfrequencies greater than 630 cycles per second the spectra are nearly identical. This is expected because the free-field spectrum shape should not change in the far field. For midfrequencies less than 630 cycles per second the spectra differ, becoming flatter as x is increased. The far-field similarity of the corrected spectra indicates that the decay fluctuations can be evaluated quantitatively with sufficient accuracy to yield corrected spectra which are good representations of true free-field spectra.

The shift of the peaks of the corrected spectra toward higher frequencies as x is increased (fig. 19) may possibly result from the general acoustic decay law for multipoles discussed in the section entitled Free Field.

An attempt to determine the ground impedance spectrum by comparing experimental loci of maximums and minimums with theoretical values proved unsuccessful, as would be expected from theoretical considerations. However, it was noted that the number of maximums and minimums occurring in a given interval of x was, at the lower frequencies, in excess of the number predicted from theory. This effect has not been explained.

SUMMARY OF RESULTS

The following results were obtained from a theoretical and experimental study of the influence of a reflecting plane on the propagation of jet noise:

Theoretical analysis: In addition to the effects already noted by Franken, it was found that:

1. The decay of noise as a function of horizontal distance from the source is only weakly dependent upon the spectrum shape.

2. The decay as a function of distance of a white spectrum is a practical representation of the decay of jet noise.

3. The filter transfer function of the acoustic receiver may have a slight effect on measured decay curves.

4. The loci of the maximums and minimums of space fluctuations of decay are functions of the receiver band width.

5. The excess acoustical path length of reflected noise over that of the direct noise produces only a negligible reduction of the average decay rate (inverse-square law).

Experimental tests: From experimental measurements of the horizontal propagation of noise at azimuths of 30° and 330° from a small air jet located 10 feet above the ground plane, it was found that:

1. The effect of ground reflections on jet-noise propagation was experimentally significant out-of-doors.

2. The decay rate of the over-all sound-pressure level as a function of distance from the source obeyed the inverse-square law (20 db/distance decade) beyond 20 feet from the source.

3. The onset of the acoustic far field occurred at approximately 10 wavelengths from the source.

4. Space fluctuations of the noise decay were measureable quantitatively. These fluctuations were as large as 10 decibels from peak to valley for 1/3-octave band width measurements.

5. The decay fluctuations were obscured for 1/3-octave bands having midfrequencies greater than 2000 cycles per second.

6. Measured jet-noise spectra could be corrected to yield corresponding free-field spectra. The shapes of corrected spectra were found to be independent of distance from the source in the far field, as predicted by theory.

7. In proceeding from the near field to the far field the frequency of the peak of the noise spectrum increased, which was in qualitative agreement with theory.

Lewis Flight Propulsion Laboratory
National Advisory Committee of Aeronautics
Cleveland, Ohio, January 15, 1958

APPENDIX A

SYMBOLS

a	speed of sound
f	frequency
f_a	lower cutoff frequency
f_b	upper cutoff frequency
f_o	acceptance frequency of pure-tone receiver
f'	$f' \equiv f - \mu$
f^*	frequency ratio, f/μ
H	receiver height above plane
h	source height above plane
k	constant mean-square pressure spectral density
m	geometric mean frequency of filter, $\sqrt{f_a f_b}$
m^*	frequency ratio, m/μ
n	a number
P	acoustic pressure at receiver
p	acoustic pressure, direct or reflected component of acoustic pressure at receiver
$p(f)$	acoustic pressure-sec, $\mathscr{R}e\int_0^T p(t)e^{-2\pi ift}\,dt$
$p^2(f_a,f_b)$	$p^2(f_a,f_b) \equiv \int_{f_a}^{f_b} p^2(f)df$
$\overline{p^2(f_a,f_b)}$	$\overline{p^2(f_a,f_b)} \equiv \frac{1}{T}\int_0^T p^2(f_a,f_b)dt$
p_o	reference pressure, 2×10^{-4} dyne-sec/cm^2
p_o'	reference pressure, 2×10^{-4} dyne/cm^2

$p(\ldots,\tau)$	acoustic pressure component at receiver via reflection path
Q	ground impedance function, $\approx \dfrac{\frac{h+H}{x} - \beta}{\frac{h+H}{x} + \beta}$ for plane waves (refs. 12 and 1)
R	ratio of mean-square acoustic pressure at receiver with plane present to free-field mean-square acoustic pressure
$\mathscr{R}$	autocorrelation coefficient
$\mathscr{R}e$	real part
r	distance from source to receiver
r_R	distance from source to receiver via reflection path
SPL	sound-pressure level
T	time period
t	time
u	$u \equiv (f - \mu)/\sigma$
v	$v \equiv (f - m)/\rho$
w	electric power
w_o	reference electric power
x	horizontal distance from source to receiver
$\lvert Y(f) \rvert^2$	steady-state power transfer function of receiver
y	$y \equiv 2\pi f\tau$
z	$z \equiv \dfrac{f}{\mu} + 1$
α	$\alpha \equiv 2\pi\mu\tau$
α'	$\alpha' \equiv 2\pi m\tau$
β	acoustic admittance ratio of plane (refs. 12 and 1)
γ	$\gamma \equiv \pi\sigma\tau$

γ'	$\gamma' \equiv \pi\rho\tau$
λ	acoustic wavelength
μ	frequency of maximum mean-square-pressure spectral density
ρ	$(-\sqrt{2})$(standard deviation of filter response curve), cps
σ	$(-\sqrt{2})$(standard deviation of mean-square-pressure spectrum), cps
σ^*	frequency ratio, σ/μ
τ	delay time
φ	directional functions
ψ	autocorrelation function

Subscripts:

a	refers to value associated with lower cutoff frequency
b	refers to value associated with upper cutoff frequency
F	far field
N	near field

Superscript:

$\bar{}$	time average

APPENDIX B

INDICATED SOUND-PRESSURE-LEVEL SPECTRA

In attempting to select an analytic expression for the mean-square-pressure spectrum which best fits experimental data, it is desirable to express the selected spectrum in the same form as the data. Usually this means that the SPL spectrum for finite band-pass widths is desired.

If the acoustic transducer responds linearly to fluctuating pressure amplitudes, the electric power output of the receiver is given by

$$w(f_a,f_b) = \int_{f_a}^{f_b} |Y(f)|^2 \overline{|p(f)|^2}\, df \qquad (B1)$$

in the pass band, where $Y(f)$ is the steady-state transfer function of the system. With ideal components (Y = const.), the indicated SPL is given by

$$\begin{aligned} SPL(f_a,f_b) &= 10 \log\left[w(f_a,f_b)/w_o\right] \\ &= 10 \log\left[\frac{1}{p_o'^2}\int_{f_a}^{f_b} \overline{|p(f)|^2}\, df\right] \end{aligned} \qquad (B2)$$

Gaussian $\overline{p^2}$ Spectrum

In dimensional form the Gaussian function becomes

$$\overline{p^2(f)} = \overline{p^2(\mu)}\, e^{-u^2}$$

Then, according to equation (B1) the electric power output of the acoustic receiver with ideal filtering (Y = const.) is given by

$$\begin{aligned} w(f_a,f_b) &= |Y|^2\, \overline{p^2(\mu)} \int_{f_a}^{f_b} e^{-u^2}\, df \\ &= |Y|^2\, \overline{p^2(\mu)}\, \sigma \int_{u_a}^{u_b} e^{-u^2}\, du \\ &= \frac{\sqrt{\pi}\sigma}{2} |Y|^2\, \overline{p^2(\mu)}\, (\operatorname{erf} u_b - \operatorname{erf} u_a) \end{aligned} \qquad (B3)$$

where, in general,

$$\operatorname{erf} U = \frac{2}{\sqrt{\pi}} \int_0^U e^{-u^2}\, du$$

The over-all electric power output is

$$w = \frac{\sqrt{\pi}\sigma}{2} |Y|^2 \overline{p^2(\mu)} \left(1 + \operatorname{erf} \frac{\mu}{\sigma}\right) \approx |Y|^2 \sqrt{\pi}\sigma \overline{p^2(\mu)} \qquad (\mu > \sigma) \qquad \text{(B3a)}$$

By virtue of equations (B2), (B3), and (B3a),

$$\mathrm{SPL}(f_a,f_b) \approx 10 \log \left(\frac{w}{w_o} \frac{\operatorname{erf} u_b - \operatorname{erf} u_a}{2}\right)$$

$$\approx \mathrm{SPL} + 10 \log (\operatorname{erf} u_b - \operatorname{erf} u_a) - 3.0 \qquad \text{(B4)}$$

where SPL is the over-all sound-pressure level.

$f^* e^{1-f^*}$ Spectrum

For a spectrum $f^* e^{1-f^*}$ and with ideal filtering

$$w(f_a,f_b) = |Y|^2 \overline{p^2(\mu)} \frac{e}{\mu} \int_{f_a}^{f_b} f e^{-f/\mu}\, df$$

$$= - |Y|^2 \overline{p^2(\mu)}\, \mu e \left[e^{-f_b/\mu}\left(\frac{f_b}{\mu} + 1\right) - e^{-f_a/\mu}\left(\frac{f_a}{\mu} + 1\right)\right] \qquad \text{(B5)}$$

so that

$$\mathrm{SPL}(f_a,f_b) = 10 \log \left[\frac{\overline{p^2}}{p_o'^2} \left(z_a e^{-f_a/\mu} - z_b e^{-f_b/\mu}\right)\right]$$

$$= \mathrm{SPL} + 10 \log \left(z_a e^{-f_a/\mu} - z_b e^{-f_b/\mu}\right) \qquad \text{(B6)}$$

where

$$w = |Y|^2 \mu e \overline{p^2(\mu)}$$

APPENDIX C

AUTOCORRELATION COEFFICIENT

The autocorrelation coefficients associated with selected spectra can be computed from

$$\mathscr{R}(f_a,f_b,\tau) = \mathscr{R}\mathscr{e}\frac{1}{\overline{p^2(f_a,f_b)}}\int_{f_a}^{f_b}\overline{p^2(f)}\ e^{2\pi i f\tau}\ df \tag{14}$$

Gaussian Spectrum

The dimensional form of the spectrum is

$$\overline{p^2(f)} = \overline{p^2(\mu)}\ e^{-u^2}$$

Unlimited band-pass width. - The autocorrelation coefficient is computed from

$$\mathscr{R}(\tau) = \mathscr{R}\mathscr{e}\int_{-\infty}^{\infty}\overline{p^2(\mu)}\ e^{-u^2}e^{2\pi i f\tau}\ df \Big/ \int_{-\infty}^{\infty}\overline{p^2(\mu)}\ e^{-u^2}\ df$$

$$= \mathscr{R}\mathscr{e}\frac{1}{\sqrt{\pi}\sigma}\int_{-\infty}^{\infty}e^{-u^2}e^{2\pi i f\tau}\ df$$

where, from appendix B,

$$w \propto \overline{p^2} = \sqrt{\pi}\sigma\ \overline{p^2(\mu)}$$

Let

$$f' = f - \mu$$

Then,

$$\mathscr{R}(\tau) = \mathscr{R}\mathscr{e}\frac{e^{2\pi i\mu\tau}}{\sqrt{\pi}\sigma}\int_{-\infty}^{\infty}e^{-f'^2/\sigma^2}e^{2\pi i f'\tau}\ df'$$

for which the solution is obtained from Fourier pair number 708.0 in reference 11. The result is

$$\mathscr{R}(\tau) = e^{-\gamma^2}\cos\alpha \tag{C1}$$

Limited band-pass width. - If the spectrum is filtered ideally,

$$\mathscr{R}(f_a,f_b,\tau) = \mathscr{R}e\frac{1}{\overline{p^2(f_a,f_b)}}\int_{f_a}^{f_b}\overline{p^2(\mu)}\ e^{-u}e^{2\pi i f\tau}\ df$$

where f_a and f_b are the lower and upper cutoff frequencies, respectively. It follows that

$$\mathscr{R}(f_a,f_b,\tau) = \mathscr{R}e\frac{2}{\sqrt{\pi}\sigma(\operatorname{erf} u_b - \operatorname{erf} u_a)}\ e^{2\pi i\mu\tau}$$

$$\int_{f_a-\mu}^{f_b-\mu} e^{-f'^2/\sigma^2}e^{2\pi i f'\tau}\ df'$$

where $\overline{p^2(f_a,f_b)}$ is extracted from equation (B3). The solution obtained from Fourier pair number 1317 in reference 11 is

$$\mathscr{R}(f_a,f_b,\tau) = \mathscr{R}e\ e^{-\gamma^2}e^{i\alpha}\frac{\operatorname{erf}(u_b - i\gamma) - \operatorname{erf}(u_a - i\gamma)}{\operatorname{erf} u_b - \operatorname{erf} u_a} \qquad (C2)$$

where the complex error functions can be computed from series expansions. The curves in figure 8 were computed from series expansions to as many as 111 terms by means of a digital computer.

$f^*e^{1-f^*}$ Spectrum

Unlimited band-pass width. - The autocorrelation coefficient is computed from

$$\mathscr{R}(\tau) = \mathscr{R}e\frac{1}{\overline{p^2}}\int_0^\infty \overline{p^2(\mu)}\ \frac{f}{\mu}\ e^{1-(f/\mu)}e^{2\pi i f\tau}\ df$$

$$= \mathscr{R}e\frac{1}{\mu^2}\int_0^\infty fe^{-f/\mu}e^{2\pi i f\tau}\ df$$

$$= \mathscr{R}e\frac{1}{\mu^2}\int_0^\infty fe^{-\zeta f}\ df$$

where, from appendix B,

$$\overline{p^2} = \mu e\overline{p^2(\mu)}$$

and

$$\zeta = \frac{1}{\mu} - 2\pi i\tau$$

Performing the indicated integration and retaining the real part result in

$$\mathscr{R}(\tau) = \frac{1 - \alpha^2}{(1 + \alpha^2)^2} \tag{C3}$$

Limited band-pass width. - With ideal filtering

$$\mathscr{R}(f_a,f_b,\tau) = \mathscr{R}e \frac{1}{\overline{p^2(f_a,f_b)}} \int_{f_a}^{f_b} \overline{p^2(\mu)}\, \frac{f}{\mu}\, e^{1-(f/\mu)} e^{2\pi i f\tau}\, df$$

$$= \mathscr{R}e \frac{-1}{\mu^2\left[e^{-f_b/\mu}\left(\frac{f_b}{\mu} + 1\right) - e^{-f_a/\mu}\left(\frac{f_a}{\mu} + 1\right)\right]}$$

$$\int_{f_a}^{f_b} f e^{-f/\mu} e^{2\pi i f\tau}\, df$$

By performing the integration and retaining the real part, the solution is

$$\begin{aligned}\mathscr{R}(f_a,f_b,\tau) = {} & \left[(1 + \alpha^2)^2\left(z_b e^{-f_b/\mu} - z_a e^{-f_a/\mu}\right)\right]^{-1} \\ & \left[(1 - \alpha^2)\left(z_b e^{-f_b/\mu}\cos y_b - z_a e^{-f_a/\mu}\cos y_a + \right.\right. \\ & y_b e^{-f_b/\mu}\sin y_b - y_a e^{-f_a/\mu}\sin y_a\Big) - \\ & 2\alpha\left(z_b e^{-f_b/\mu}\sin y_b - z_a e^{-f_a/\mu}\sin y_a - \right. \\ & \left.\left. y_b e^{-f_b/\mu}\cos y_b + y_a e^{-f_a/\mu}\cos y_a\right)\right]\end{aligned} \tag{C4}$$

where

$$z_a = \frac{f_a}{\mu} + 1 \qquad z_b = \frac{f_b}{\mu} + 1$$

$$y_a = 2\pi f_a \tau \qquad y_b = 2\pi f_b \tau$$

White Spectrum

A white spectrum is given by

$$\overline{p^2(f)} = k = \text{const.}$$

Unlimited band-pass width. - The autocorrelation coefficient is computed from

$$\mathscr{R}(\tau) = \mathscr{R}e \frac{1}{\overline{p^2}} \int_0^\infty k e^{2\pi i f \tau} \, df$$

where

$$\overline{p^2} = \int_0^\infty k \, df$$

Therefore,

$$\mathscr{R}(\tau) = 0 \qquad (\tau \neq 0) \tag{C5}$$

Limited band-pass width. - With ideal filtering,

$$\mathscr{R}(f_a, f_b, \tau) = \mathscr{R}e \frac{1}{\overline{p^2(f_a, f_b)}} \int_{f_a}^{f_b} k e^{2\pi i f \tau} \, df$$

where

$$\overline{p^2(f_a, f_b)} = k(f_b - f_a)$$

Therefore,

$$\mathscr{R}(f_a, f_b, \tau) = \frac{1}{2\pi\tau(f_b - f_a)} (\sin 2\pi f_b \tau - \sin 2\pi f_a \tau)$$

$$= \frac{\sin\left[\pi(f_b - f_a)\tau\right]}{\pi(f_b - f_a)\tau} \cos\left[\pi(f_b + f_a)\tau\right] \tag{C6a}$$

$$(\tau \neq 0)$$

and

$$\mathscr{R}(f_a,f_b,0) = 1 \tag{C6b}$$

Nonideal filtering. - By applying equation (B1), a white spectrum subjected to a Gaussian filter transfer function yields an output

$$w = \int_{-\infty}^{\infty} ke^{-v^2}\,df \approx \sqrt{\pi}k\rho$$

where

$$v = \frac{f - m}{\rho}$$

and m and ρ are filter, not spectrum, characteristics. The autocorrelation coefficient is computed from

$$\mathscr{R}(\tau) = \mathscr{R}_{\mathscr{L}} \int_{-\infty}^{\infty} ke^{-v^2}e^{2\pi if\tau}\,df \Big/ \sqrt{\pi}k\rho$$

which, with the exception of the constants, is identical to the autocorrelation coefficient for an unfiltered Gaussian spectrum. Therefore, the solution is

$$\mathscr{R}(\tau) = e^{-\gamma'^2}\cos\alpha' \tag{C7}$$

REFERENCES

1. Franken, Peter A.: A Theoretical Analysis of the Field of a Random Noise Source Above an Infinite Plane. NACA TN 3557, 1955.

2. Callaghan, Edmund E., and Coles, Willard D.: Far Noise Field of Air Jets and Jet Engines. NACA Rep. 1329, 1957. (Supersedes NACA TN's 3590 and 3591.)

3. Lighthill, M. J.: On Sound Generated Aerodynamically. I - General Theory. Proc. Roy. Soc. (London), ser. A, vol. 211, no. 1107, Mar. 20, 1952, pp. 564-587.

4. Lighthill, M. J.: On Sound Generated Aerodynamically. II - Turbulence as a Source of Sound. Proc. Roy. Soc. (London), ser. A, vol. 222, no. 1148, Feb. 23, 1954, pp. 1-32.

5. Howes, Walton L., Callaghan, Edmund E., Coles, Willard D., and Mull, Harold R.: Near Noise Field of a Jet-Engine Exhaust. NACA Rep. 1338, 1957. (Supersedes NACA TN's 3763 and 3764.)

6. Ingard, Uno: Review of the Influence of Meteorological Conditions on Sound Propagation. Jour. Acous. Soc. Am., vol. 25, no. 3, May 1953, pp. 405-411.

7. Greatrex, F. B.: Jet Noise. Preprint No. 559, Inst. Aero. Sci., 1955.

8. Tyler, John M., and Perry, Edward C.: Jet Noise. Preprint No. 287, SAE, 1954.

9. Mawardi, Osman K.: On the Spectrum of Noise from Turbulence. Jour. Acous. Soc. Am., vol. 27, no. 3, May 1955, pp. 442-445.

10. Bennett, W. R.: Methods of Solving Noise Problems. Proc. IRE, vol. 44, no. 5, May 1956, pp. 609-638. (See also Monograph 2624, Tech. Pub., Bell Telephone System, 1956.)

11. Campbell, George A., and Foster, Ronald M.: Fourier Integrals for Practical Applications. D. Van Nostrand Co., Inc., 1948.

12. Ingard, Uno: On the Reflection of a Spherical Sound Wave from an Infinite Plane. Jour. Acous. Soc. Am., vol. 23, no. 3, May 1951, pp. 329-335.

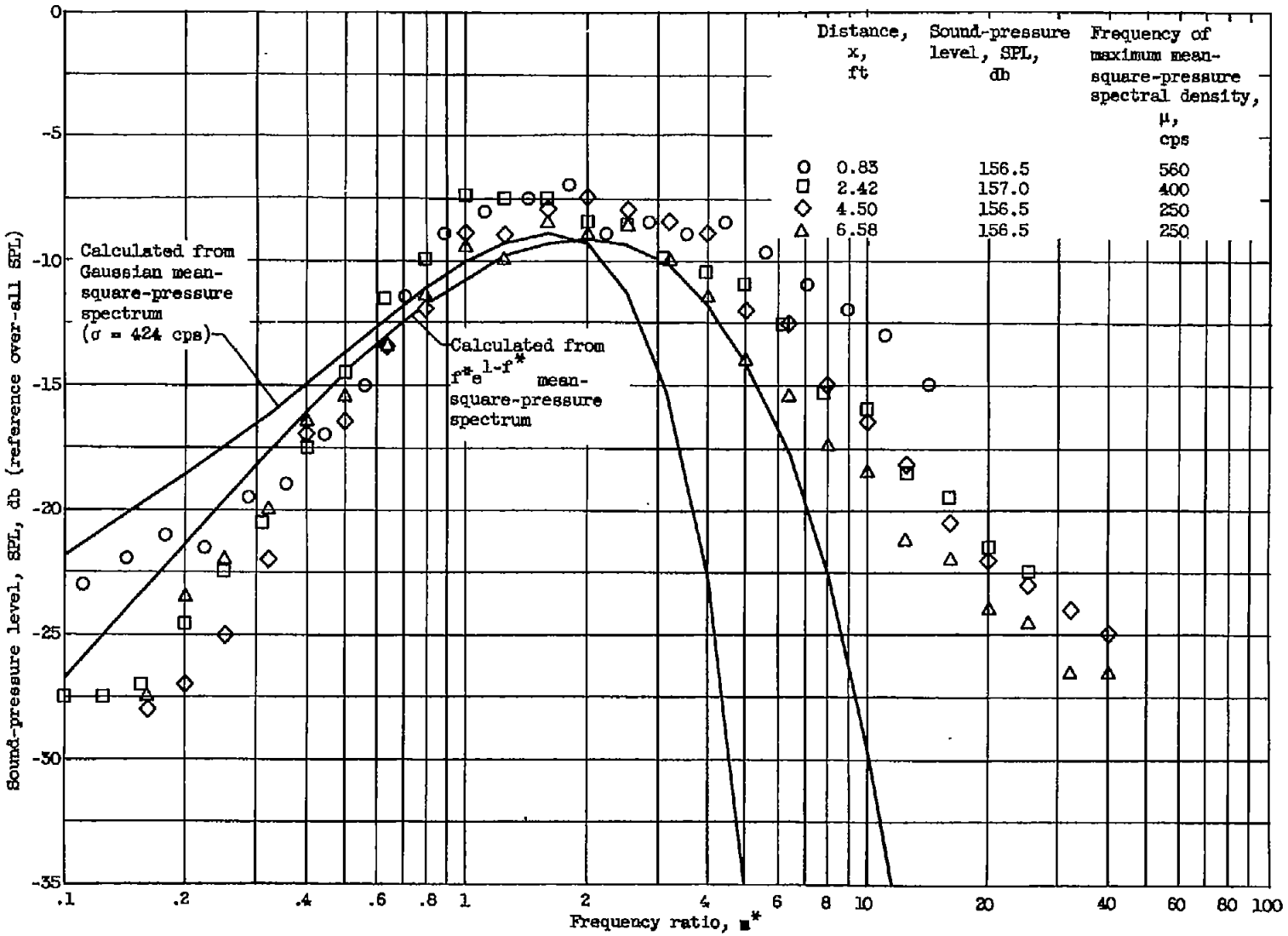

Figure 1. - Dimensionless 1/3-octave sound-pressure-level spectra along jet-engine-exhaust boundary (ref. 5).

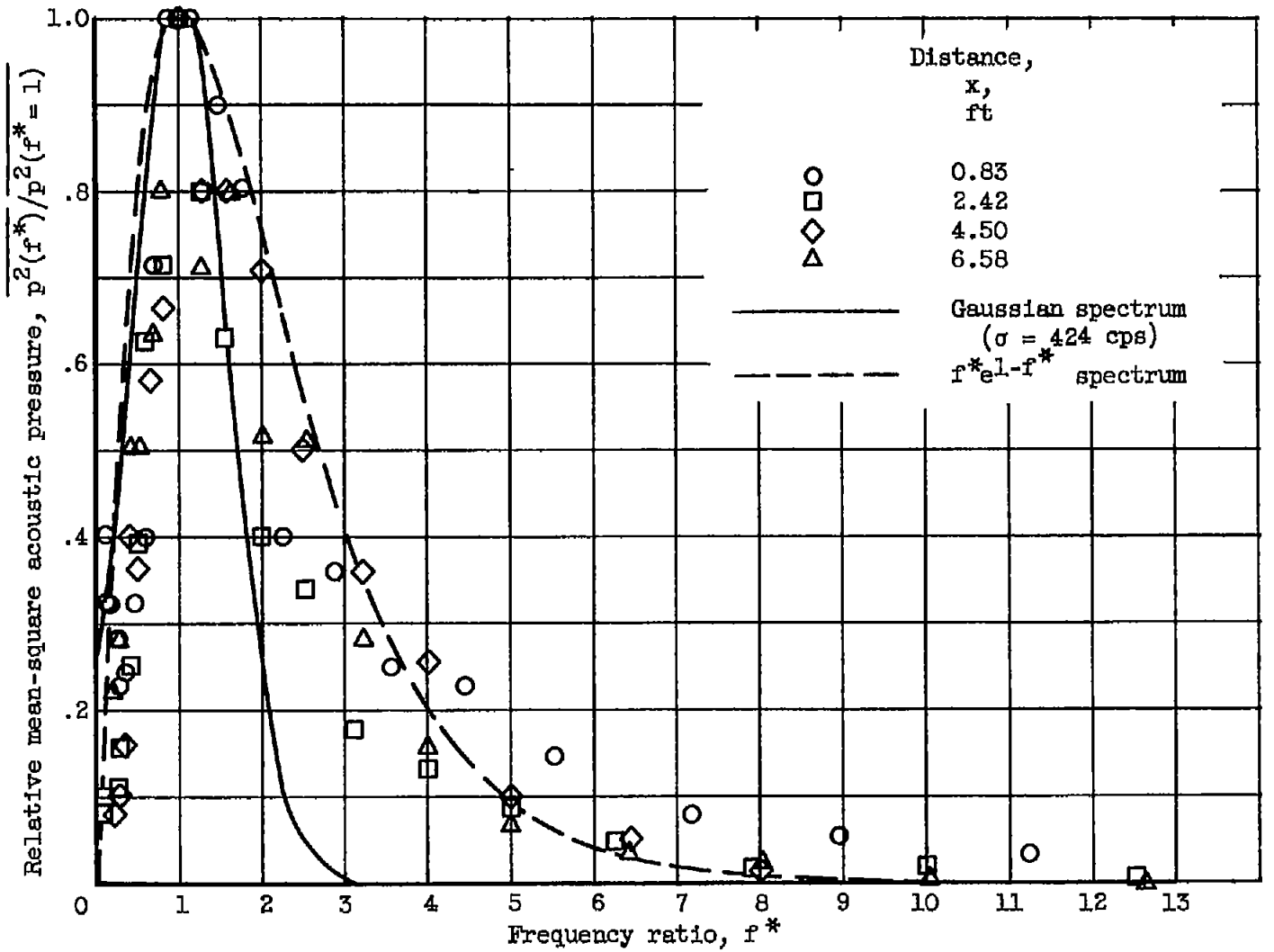

Figure 2. - Dimensionless relative mean-square-acoustic-pressure spectra along jet-engine-exhaust boundary.

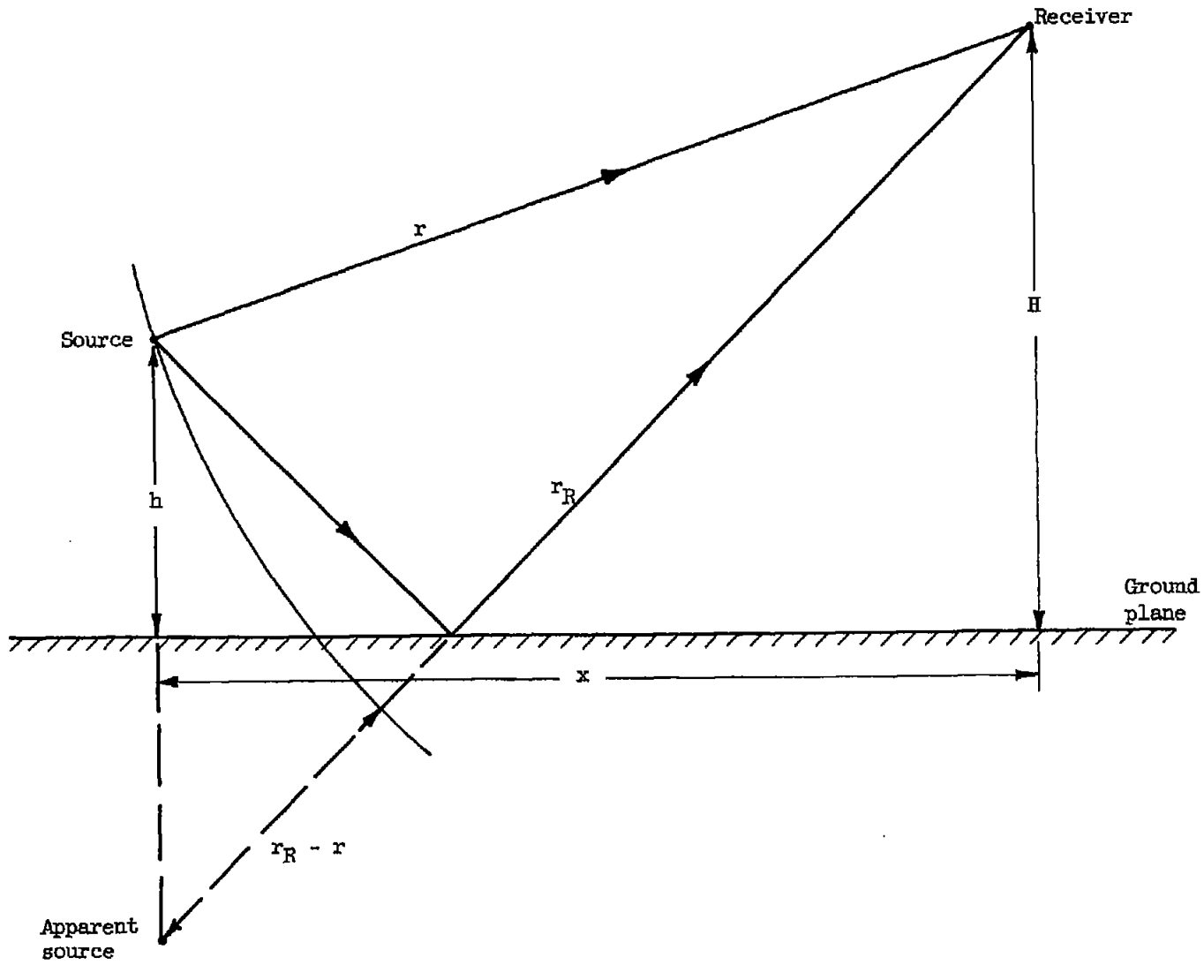

Figure 3. - Geometry of noise field in presence of plane reflector.

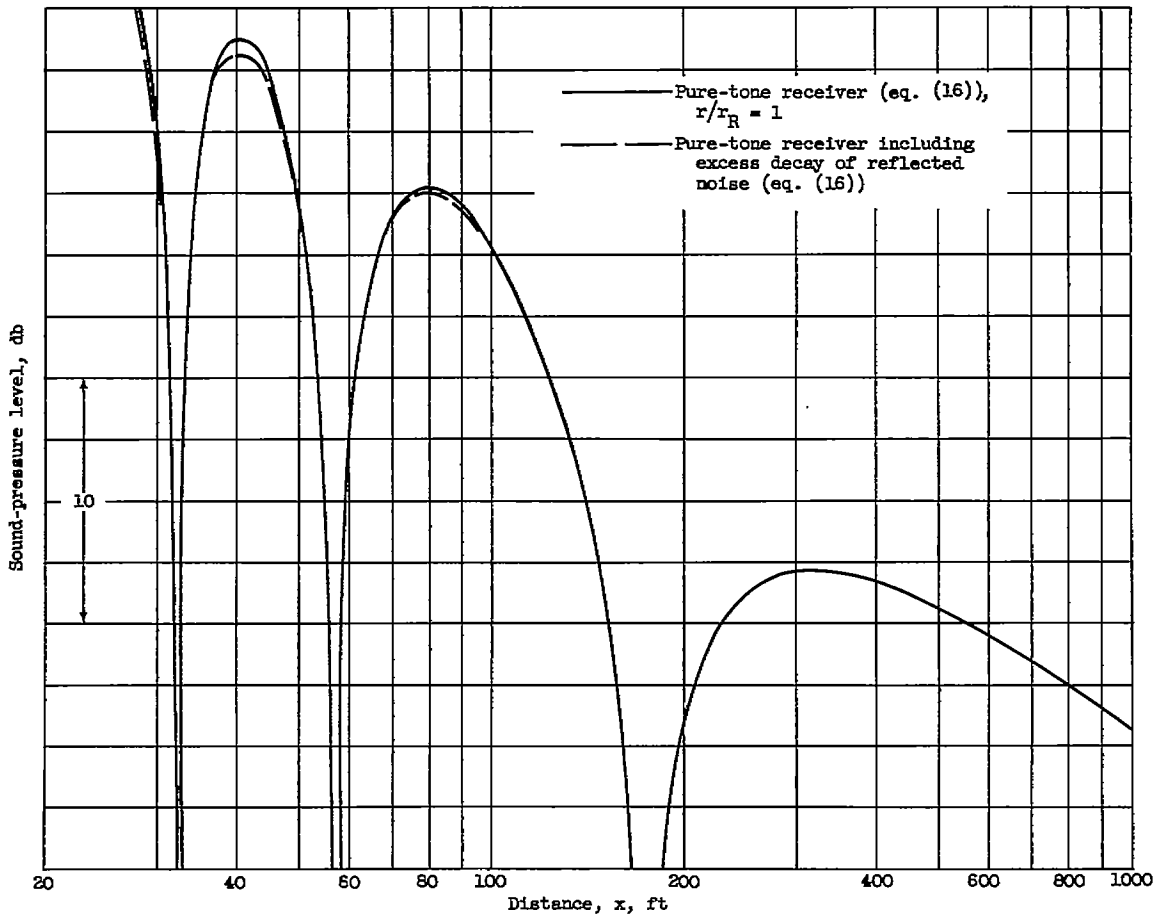

Figure 4. - Effect of excess decay of reflected noise. Pure-tone receiver; perfect reflector; acceptance frequency, 500 cycles per second; source and receiver heights above plane, 10 feet; speed of sound, 1140 feet per second.

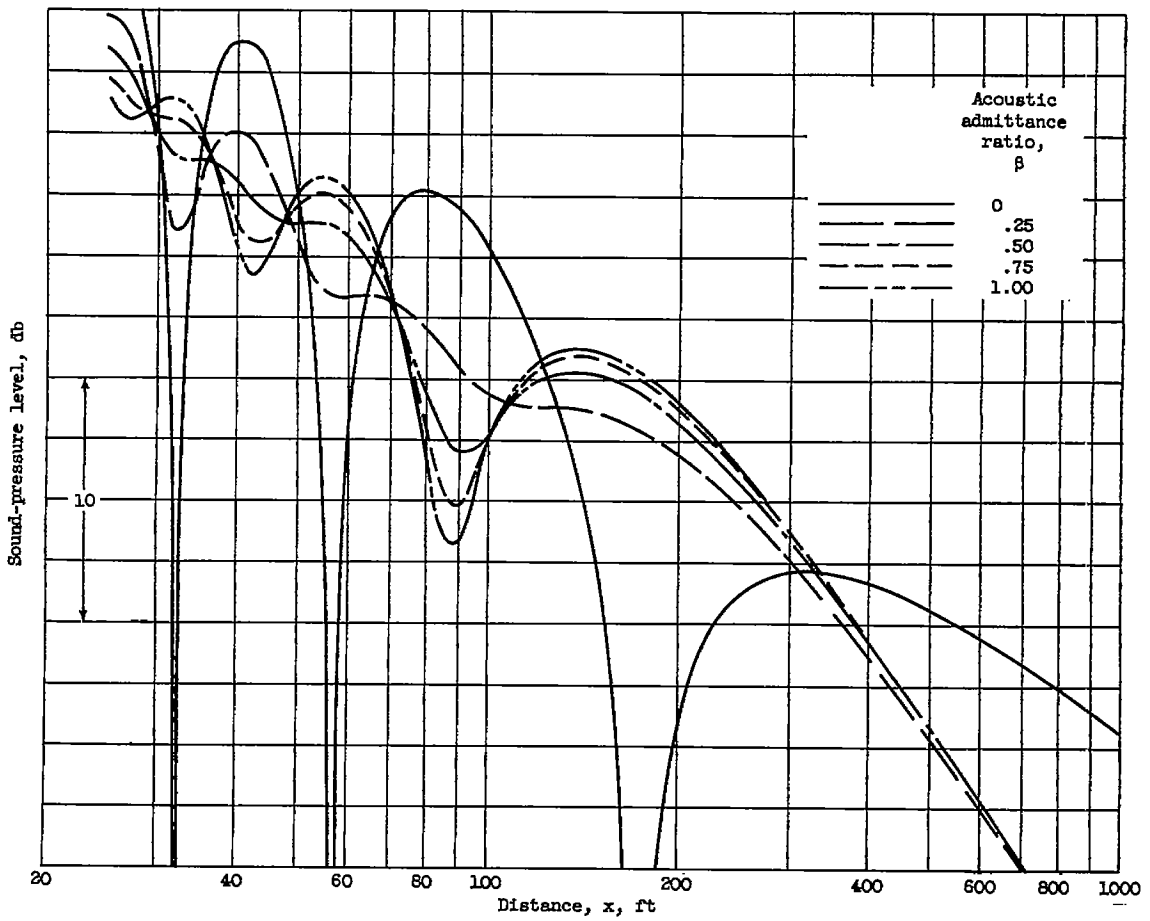

Figure 5. - Effect of varying ground impedance on decay. Pure-tone receiver (eq. (17)); acceptance frequency, 500 cycles per second; source and receiver heights above plane, 10 feet; speed of sound, 1140 feet per second.

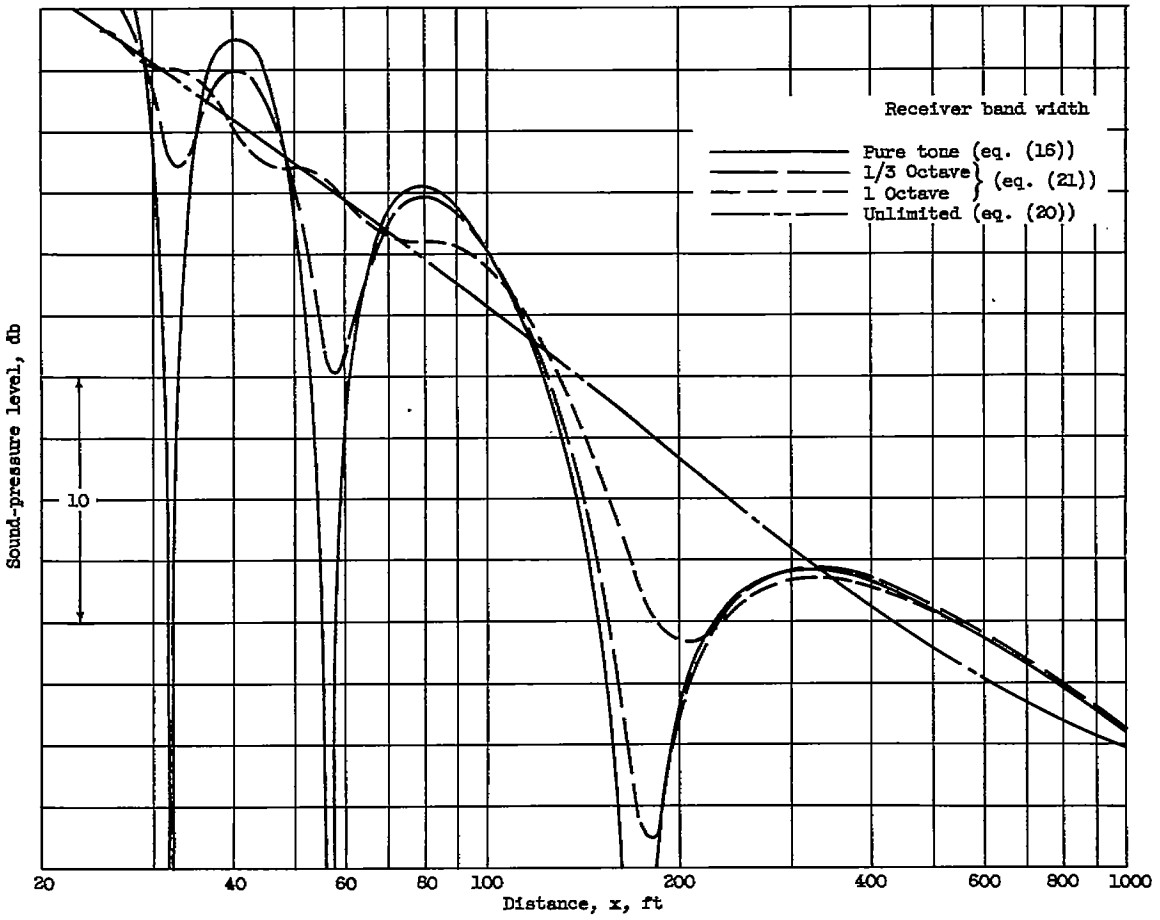

Figure 6. - Effect of receiver band width on decay of $f^{*}e^{1-f^{*}}$ spectrum. Perfect reflector; spectral-density-peak and mean filter frequencies, 500 cycles per second; source and receiver heights above plane, 10 feet; speed of sound, 1140 feet per second.

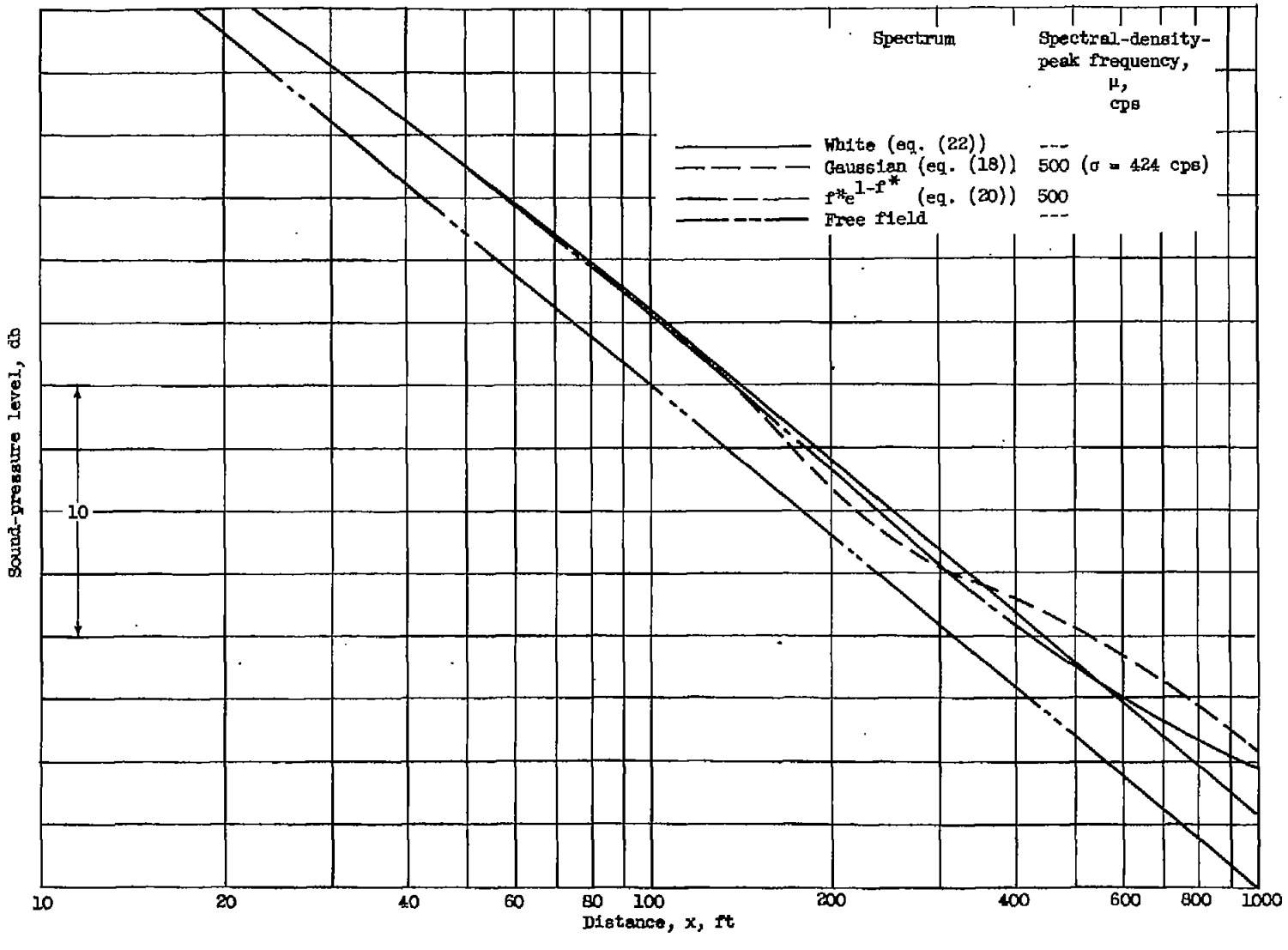

Figure 7. - Effect of spectrum shape on decay for unlimited band pass. Perfect reflector; source and receiver heights above plane, 10 feet; speed of sound, 1140 feet per second.

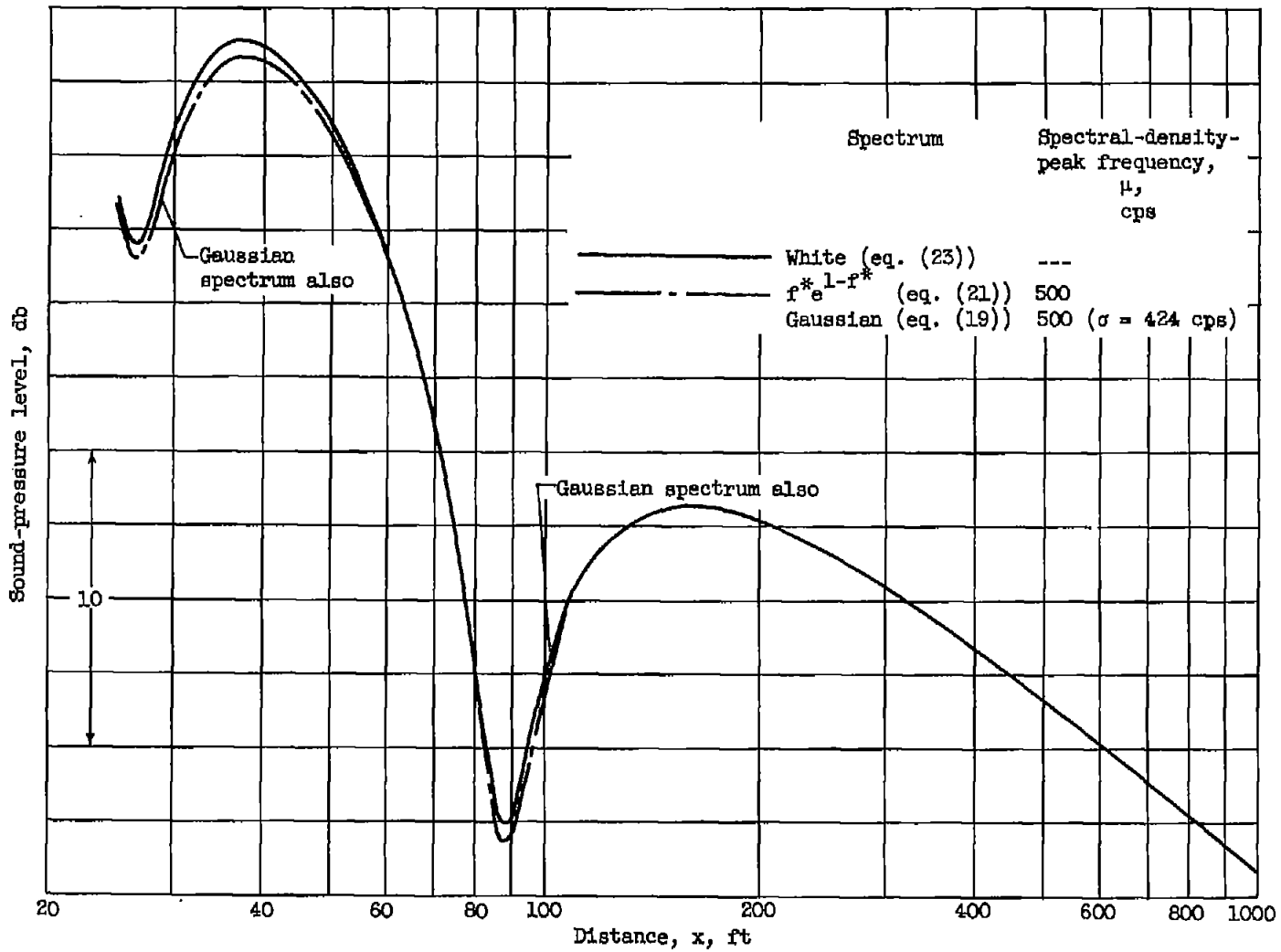

(a) Lower cutoff frequency, 224 cycles per second; upper cutoff frequency, 280 cycles per second.

Figure 8. - Effect of spectrum shape on decay for 1/3-octave receiver. Perfect reflector; source and receiver heights above plane, 10 feet; speed of sound, 1140 feet per second.

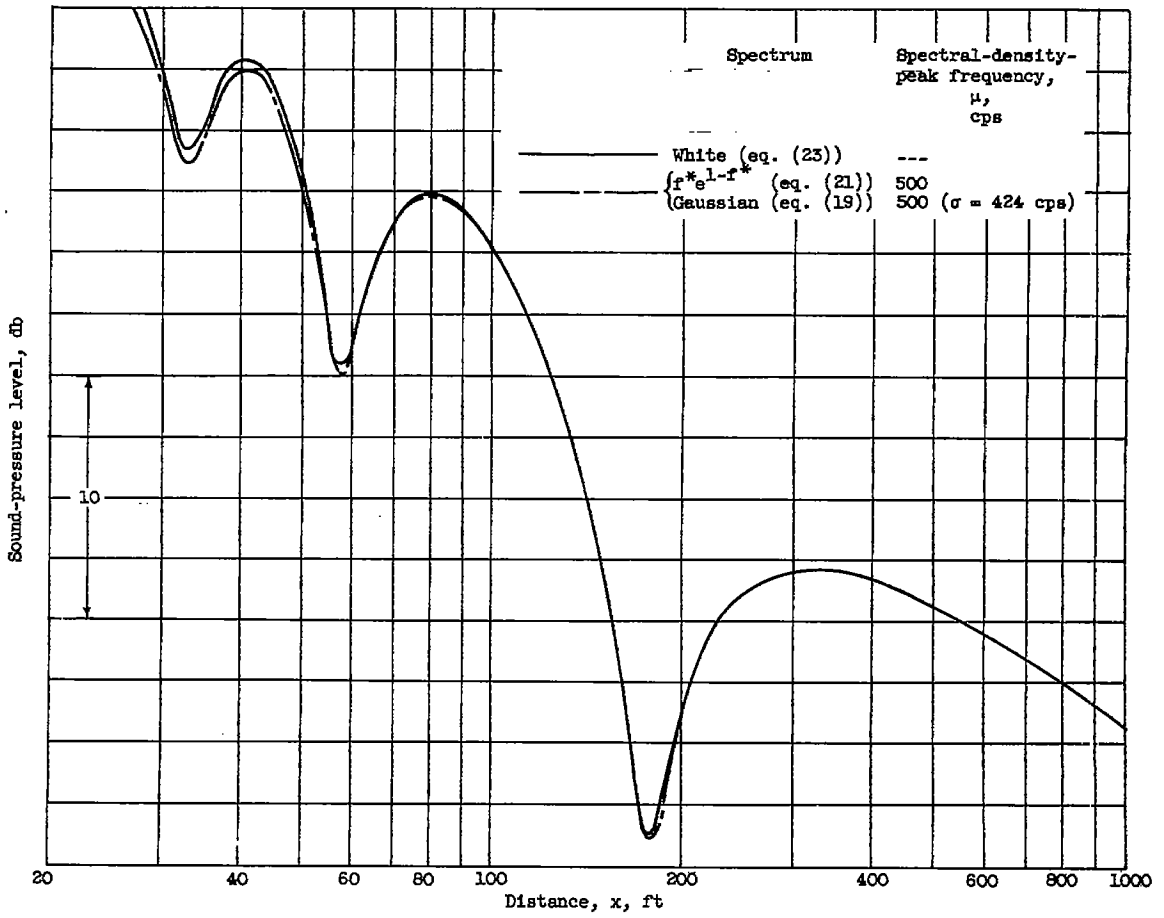

(b) Lower cutoff frequency, 447 cycles per second; upper cutoff frequency, 562 cycles per second.

Figure 8. - Continued. Effect of spectrum shape on decay for 1/3-octave receiver. Perfect reflector; source and receiver heights above plane, 10 feet; speed of sound, 1140 feet per second.

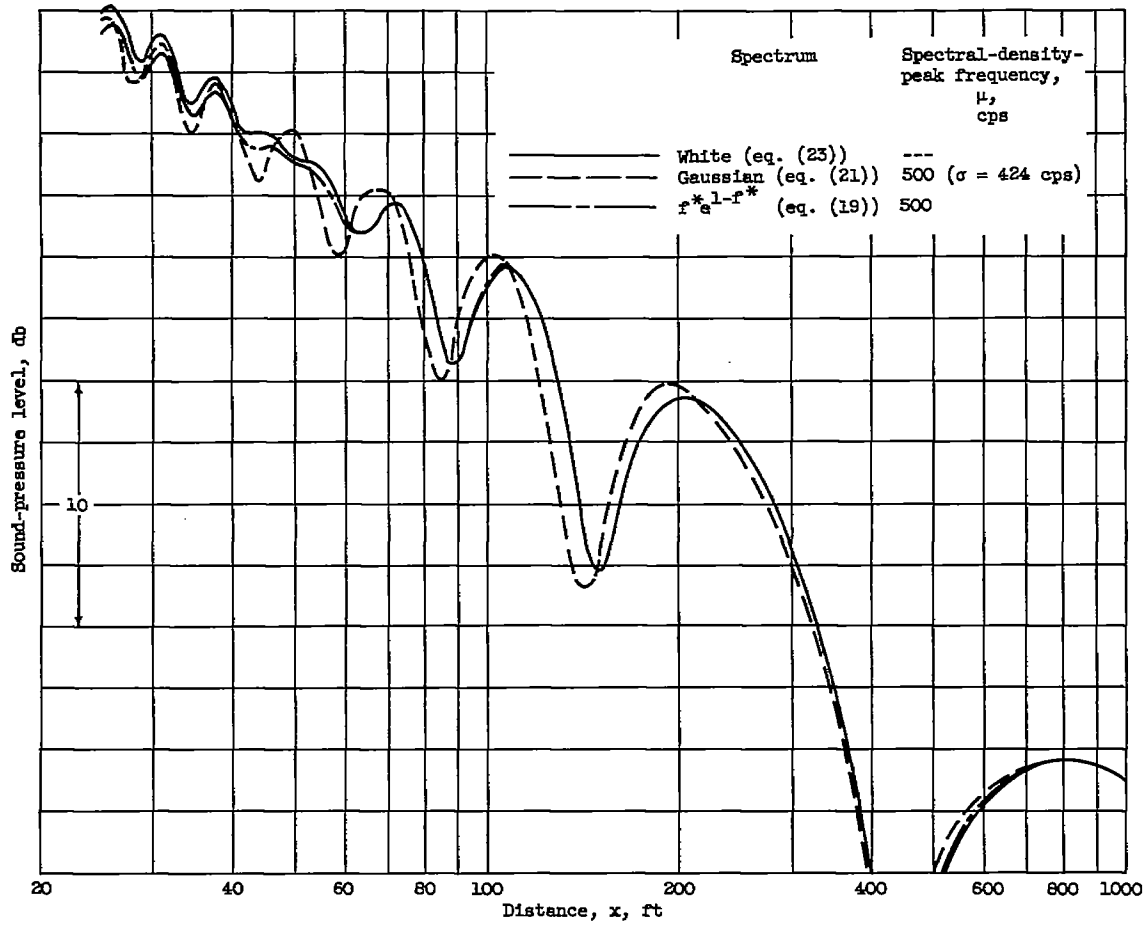

(c) Lower cutoff frequency, 1122 cycles per second; upper cutoff frequency, 1412 cycles per second.

Figure 8. - Concluded. Effect of spectrum shape on decay for 1/3-octave receiver. Perfect reflector; source and receiver heights above plane, 10 feet; speed of sound, 1140 feet per second.

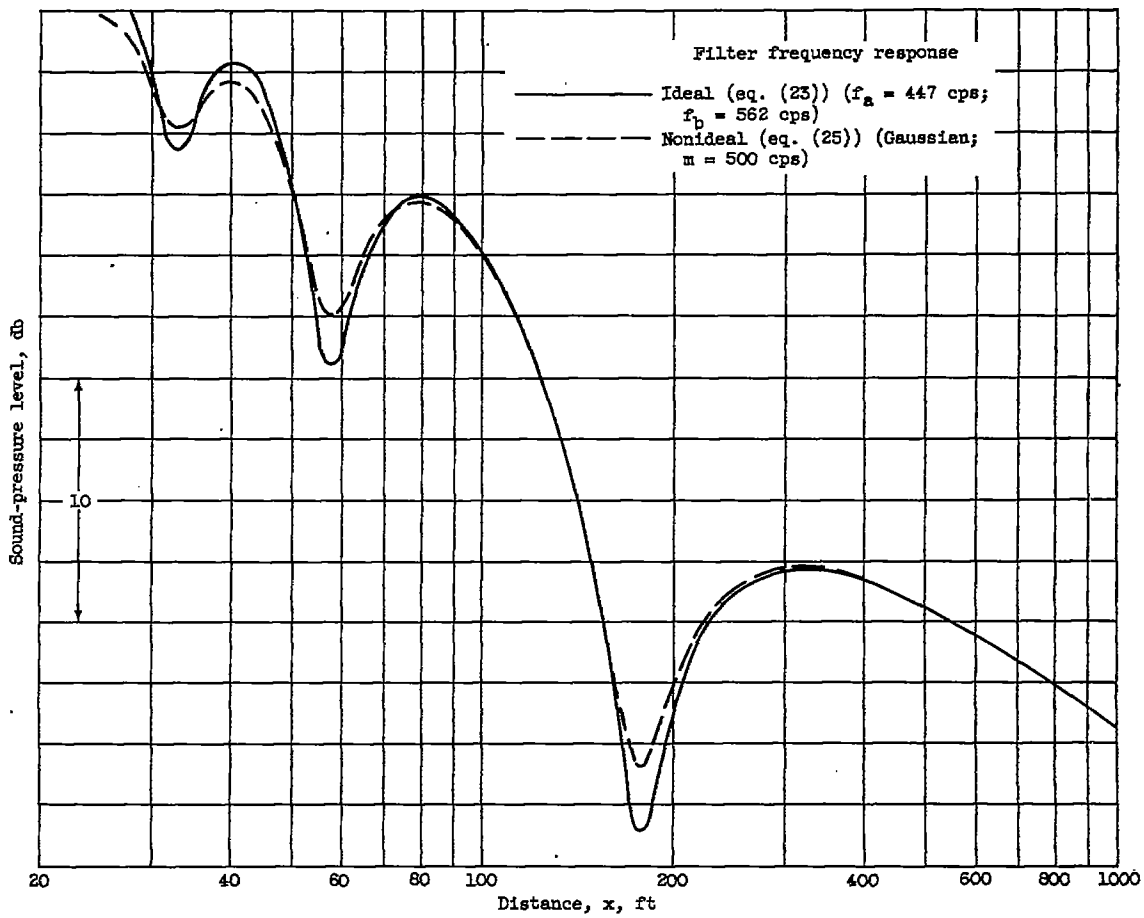

Figure 9. - Effect of filter frequency response on measured decay. White spectrum; 1/3-octave receiver; source and receiver heights from plane, 10 feet; speed of sound, 1140 feet per second.

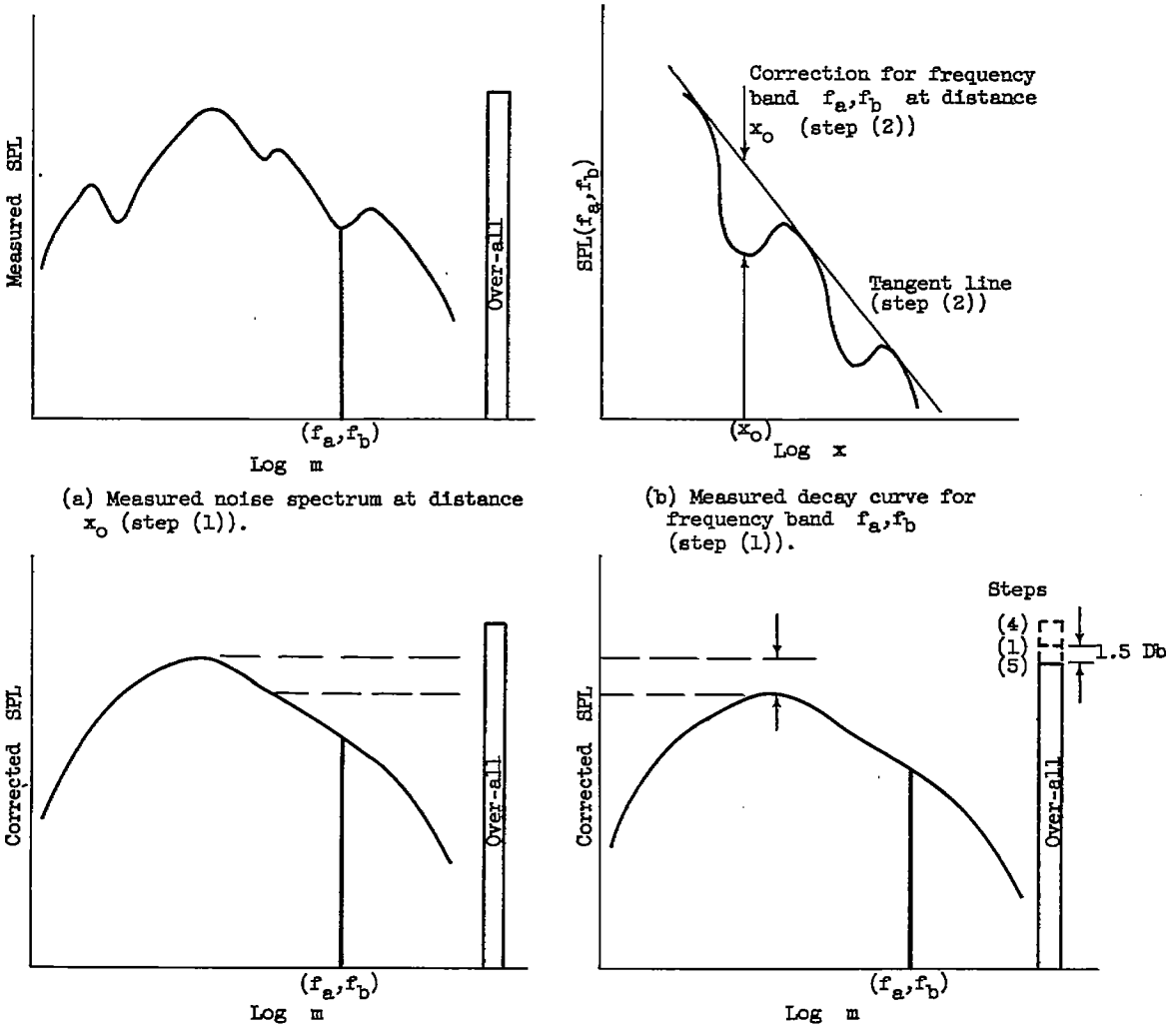

(a) Measured noise spectrum at distance x_o (step (1)).

(b) Measured decay curve for frequency band f_a,f_b (step (1)).

(c) Corrected spectrum (step (3)).

(d) Corrected spectrum (step (5)).

Figure 10. - Steps in procedure for correcting spectrum for reflection effects.

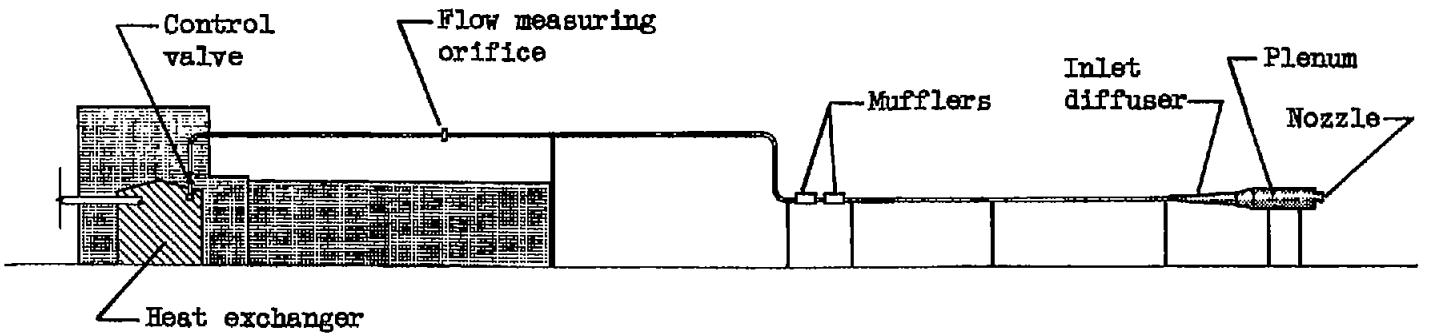

(a) Elevation.

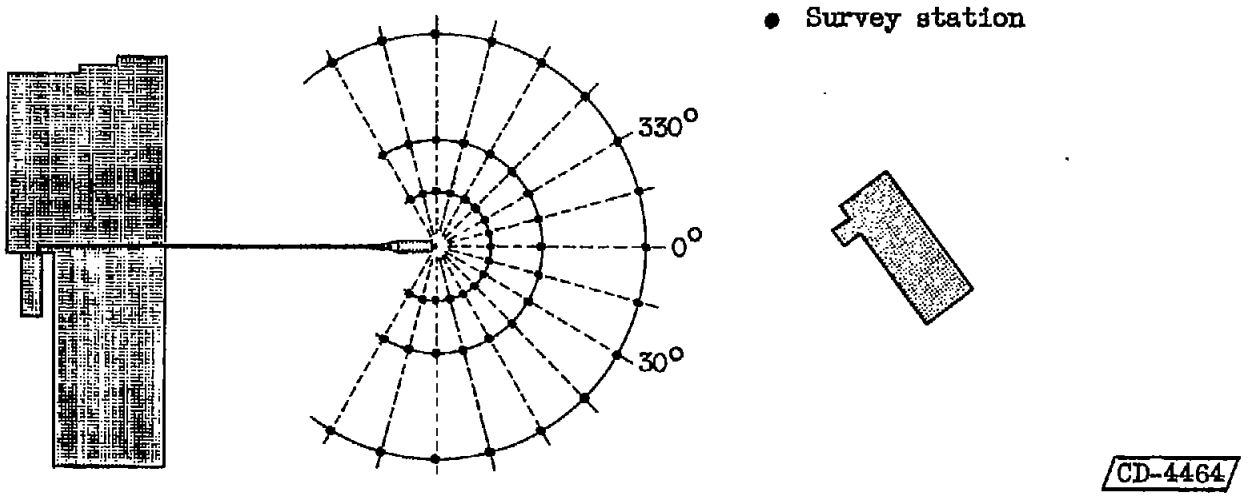

(b) Plan view of air-jet system and adjacent buildings.

Figure 11. - Air-jet facility.

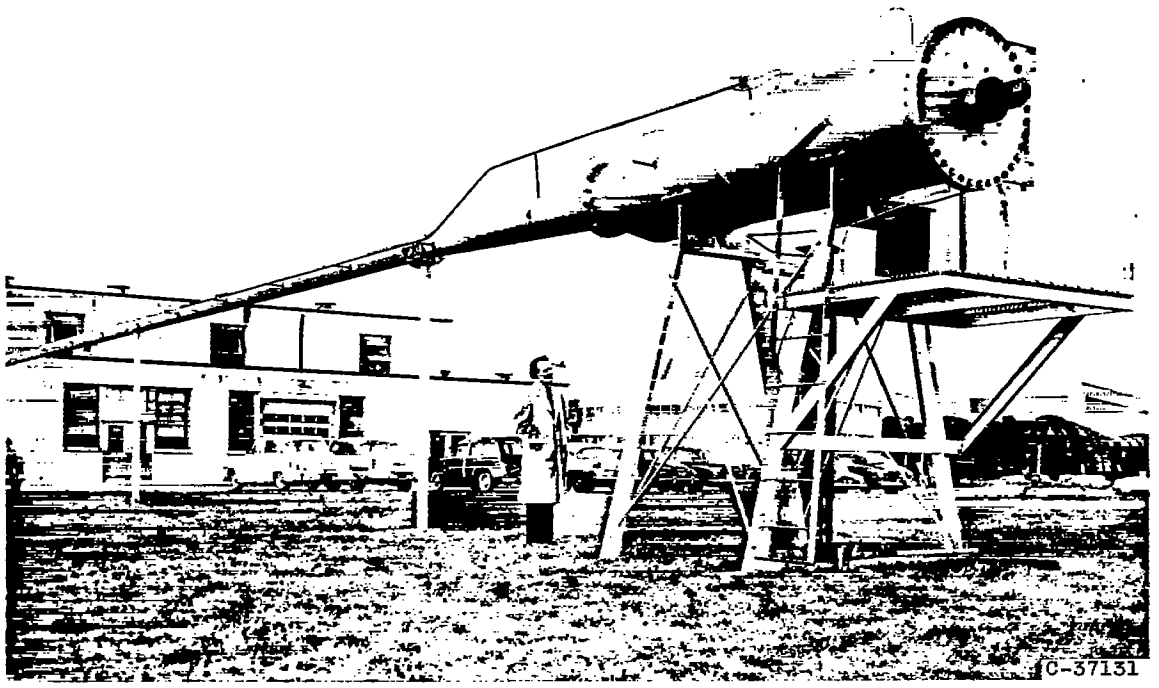

(c) Photograph of air-jet system.

Figure 11. - Concluded. Air-jet facility.

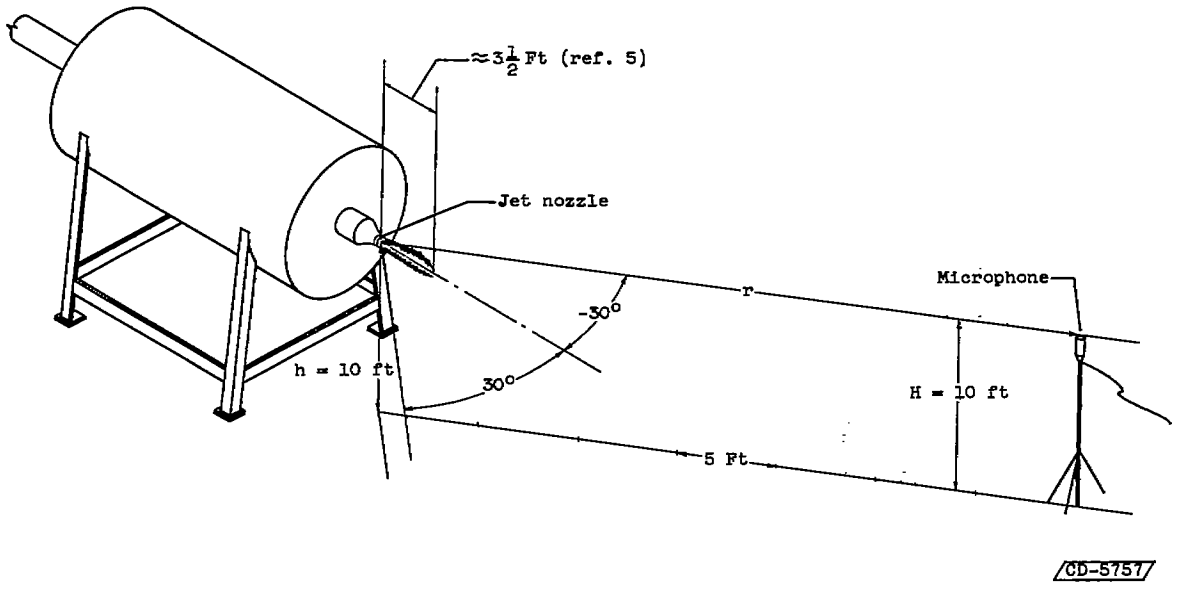

Figure 12. - Experimental geometry.

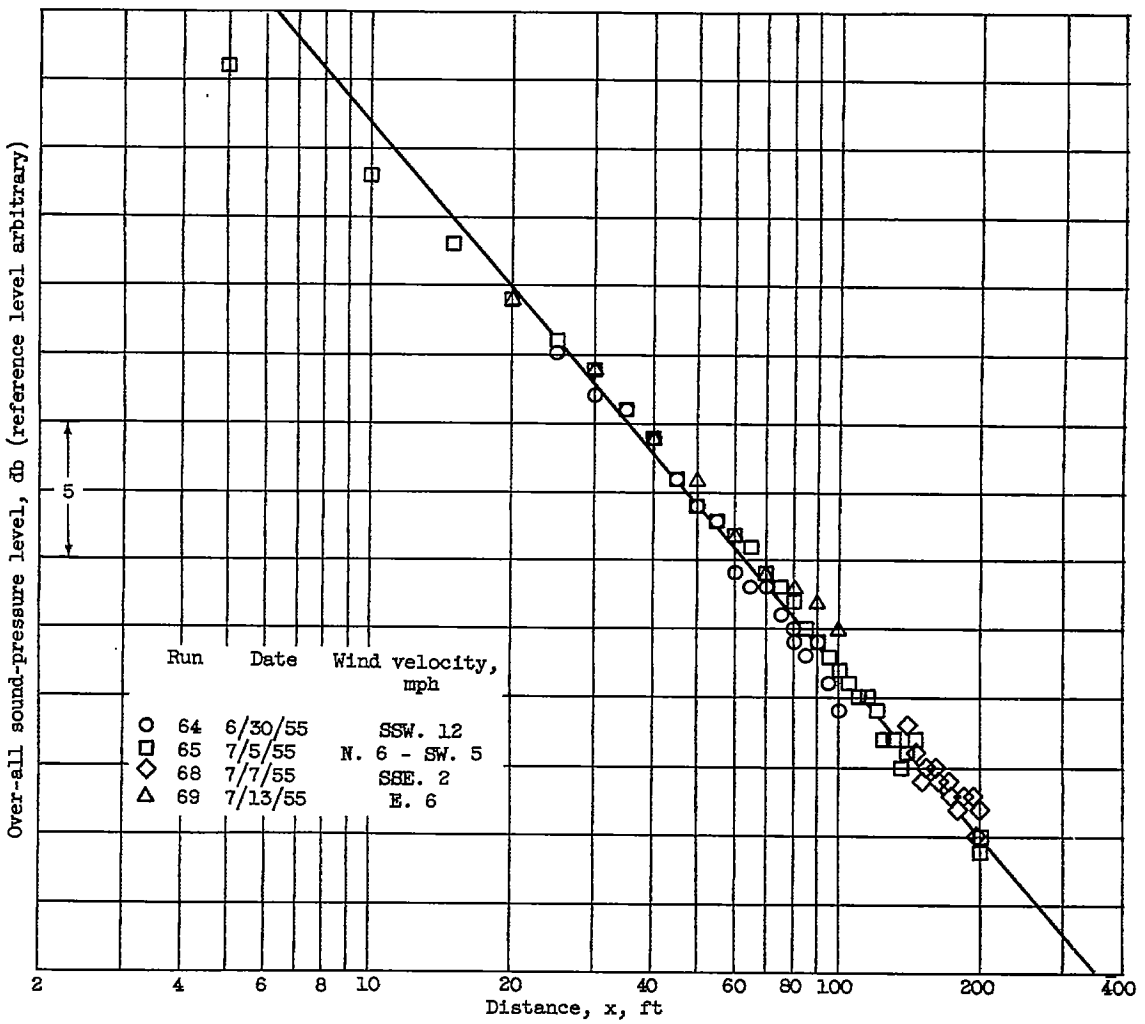

Figure 13. - Decay of over-all sound-pressure level. Source and receiver heights above plane, 10 feet; azimuth, 30° or 330°.

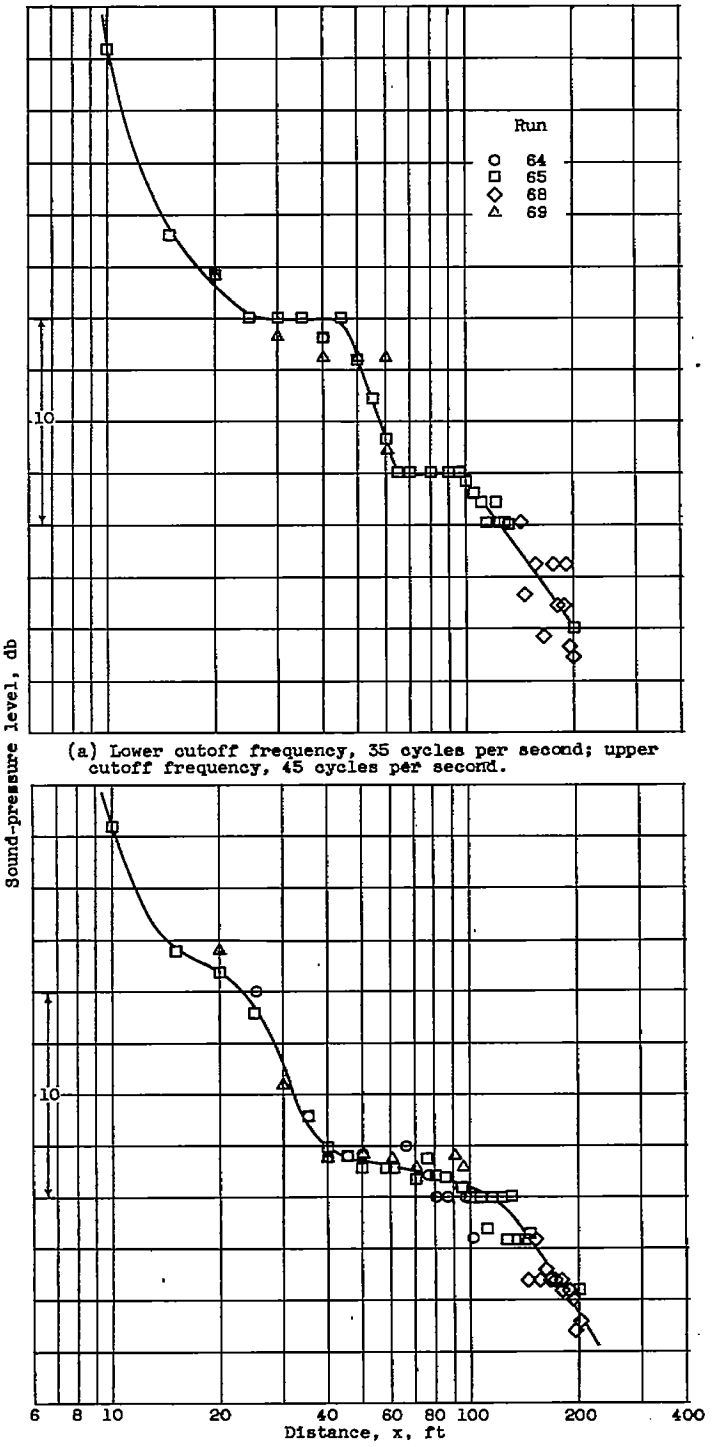

(a) Lower cutoff frequency, 35 cycles per second; upper cutoff frequency, 45 cycles per second.

(b) Lower cutoff frequency, 89 cycles per second; upper cutoff frequency, 112 cycles per second.

Figure 14. - Decay of sound-pressure level for 1/3-octave band widths. Source and receiver heights, 10 feet; azimuth, 30° or 330°.

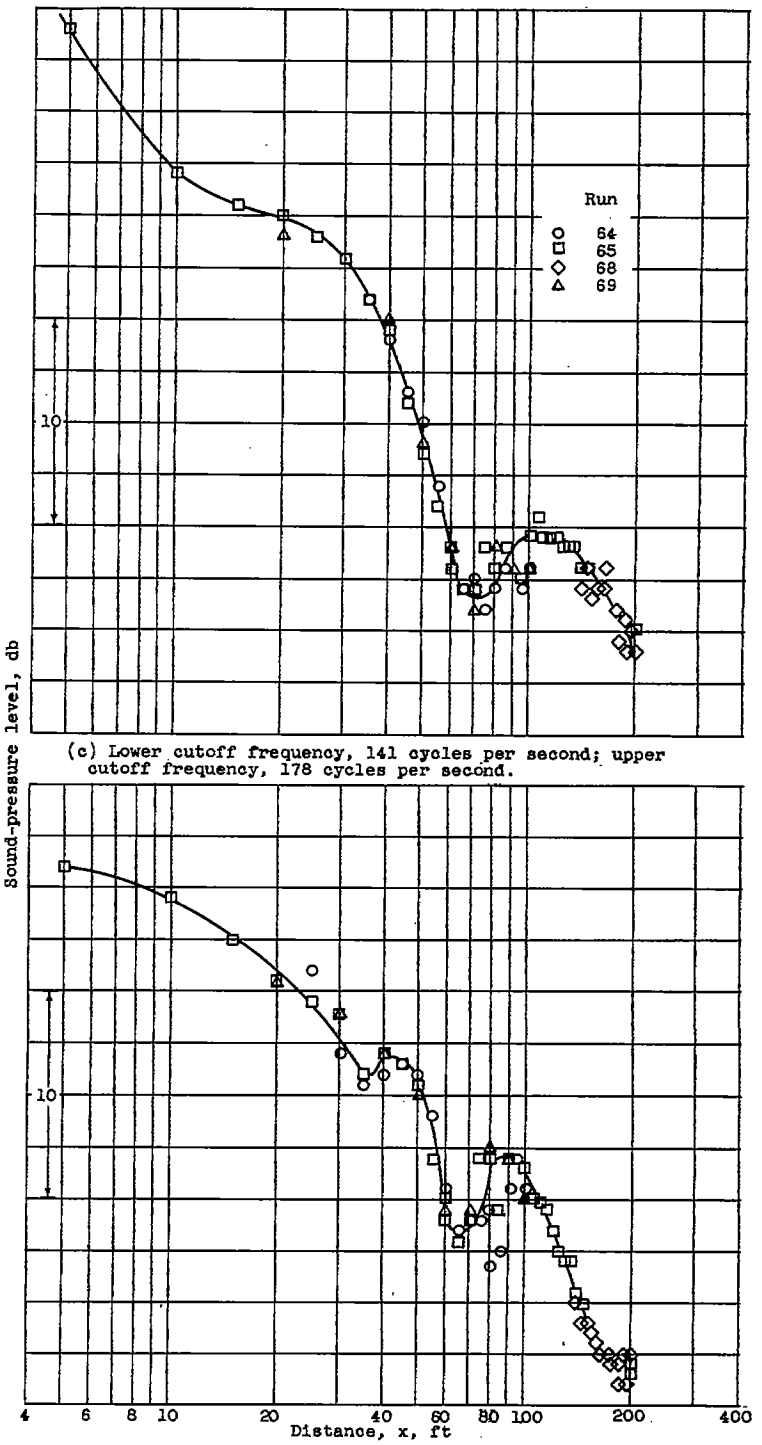

(c) Lower cutoff frequency, 141 cycles per second; upper cutoff frequency, 178 cycles per second.

(d) Lower cutoff frequency, 447 cycles per second; upper cutoff frequency, 562 cycles per second.

Figure 14. - Continued. Decay of sound-pressure level for 1/3-octave band widths. Source and receiver heights, 10 feet; azimuth, 30° or 330°.

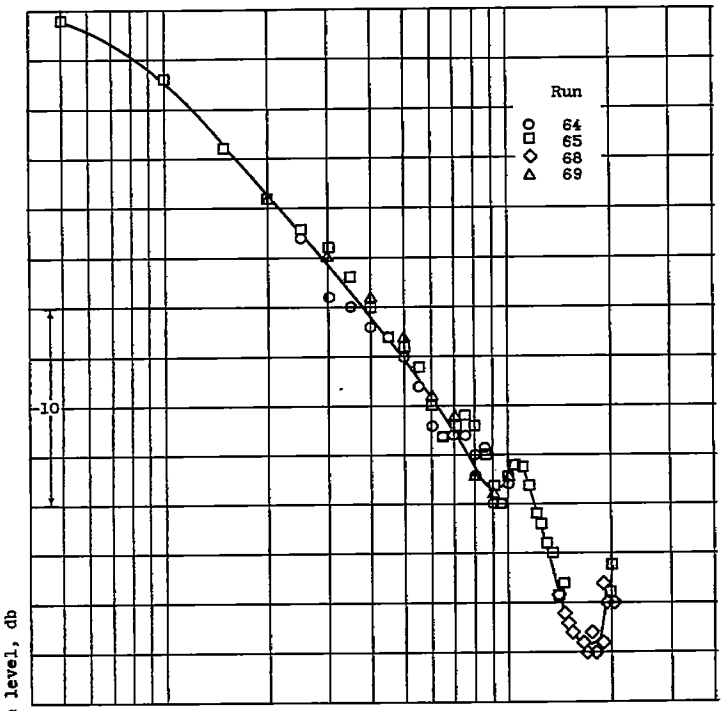

(e) Lower cutoff frequency, 1120 cycles per second; upper cutoff frequency, 1410 cycles per second.

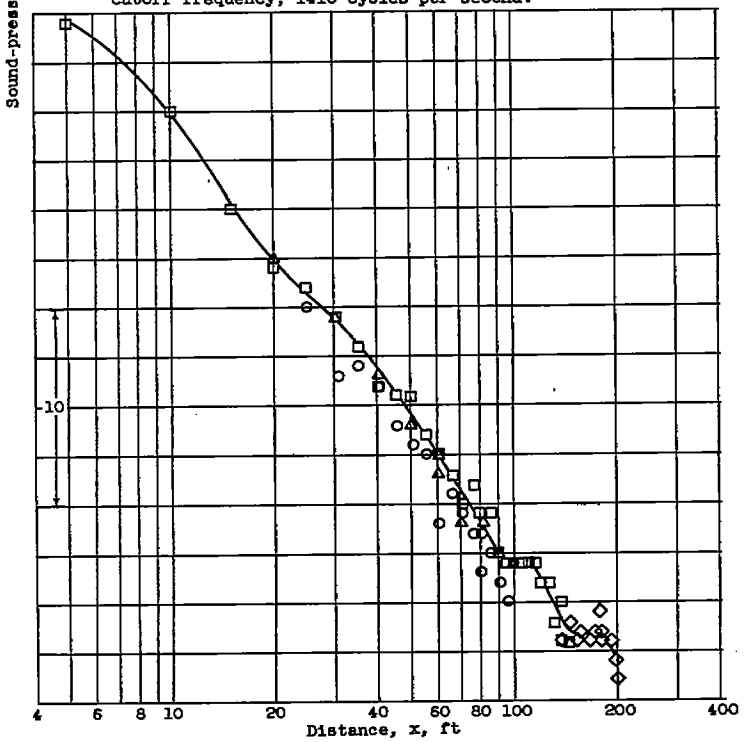

(f) Lower cutoff frequency, 1780 cycles per second; upper cutoff frequency, 2240 cycles per second.

Figure 14. - Concluded. Decay of sound-pressure level for 1/3-octave band widths. Source and receiver heights, 10 feet; azimuth, 30° or 330°.

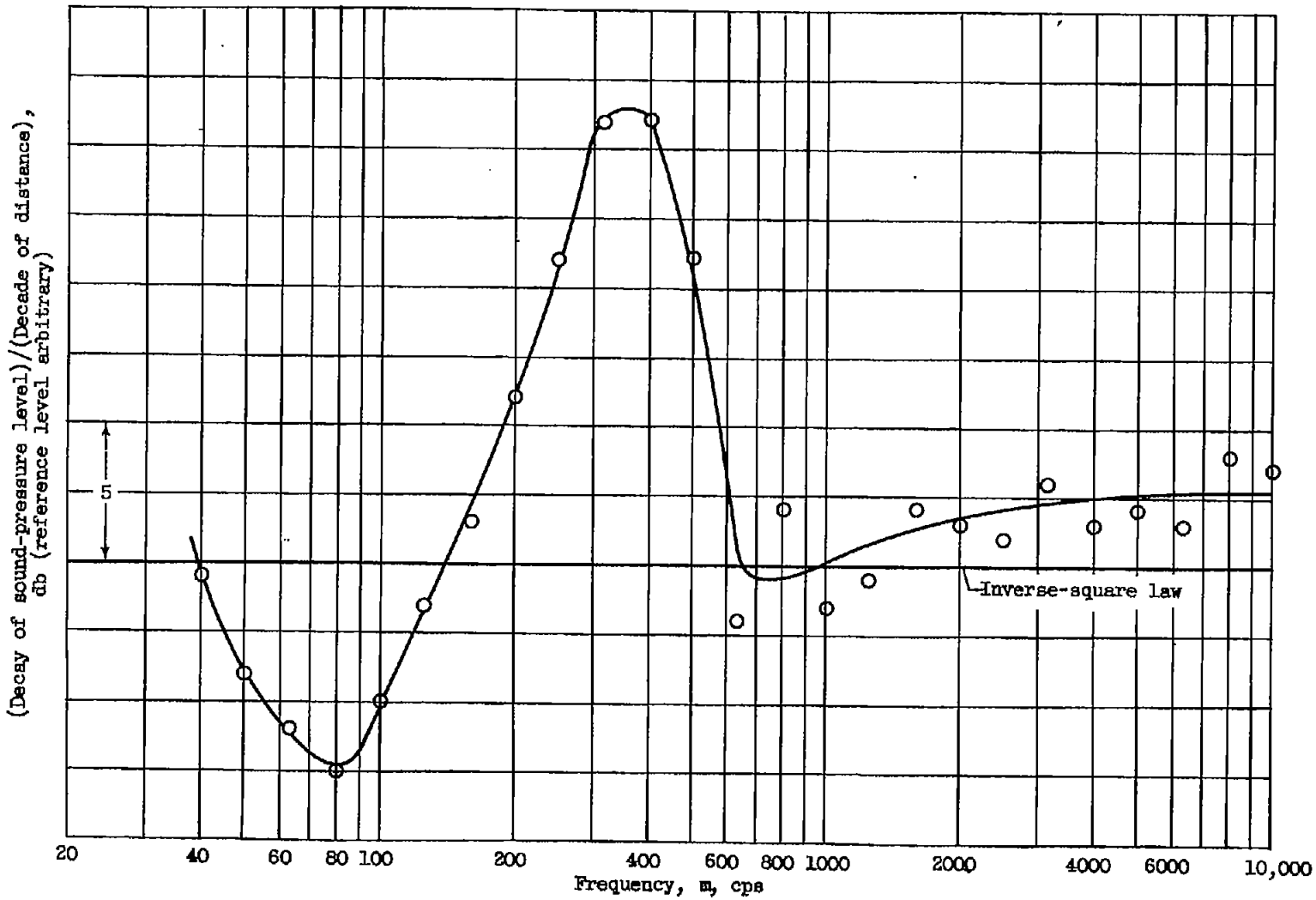

Figure 15. - Average sound-pressure-level decay rates in 1/3-octave bands.

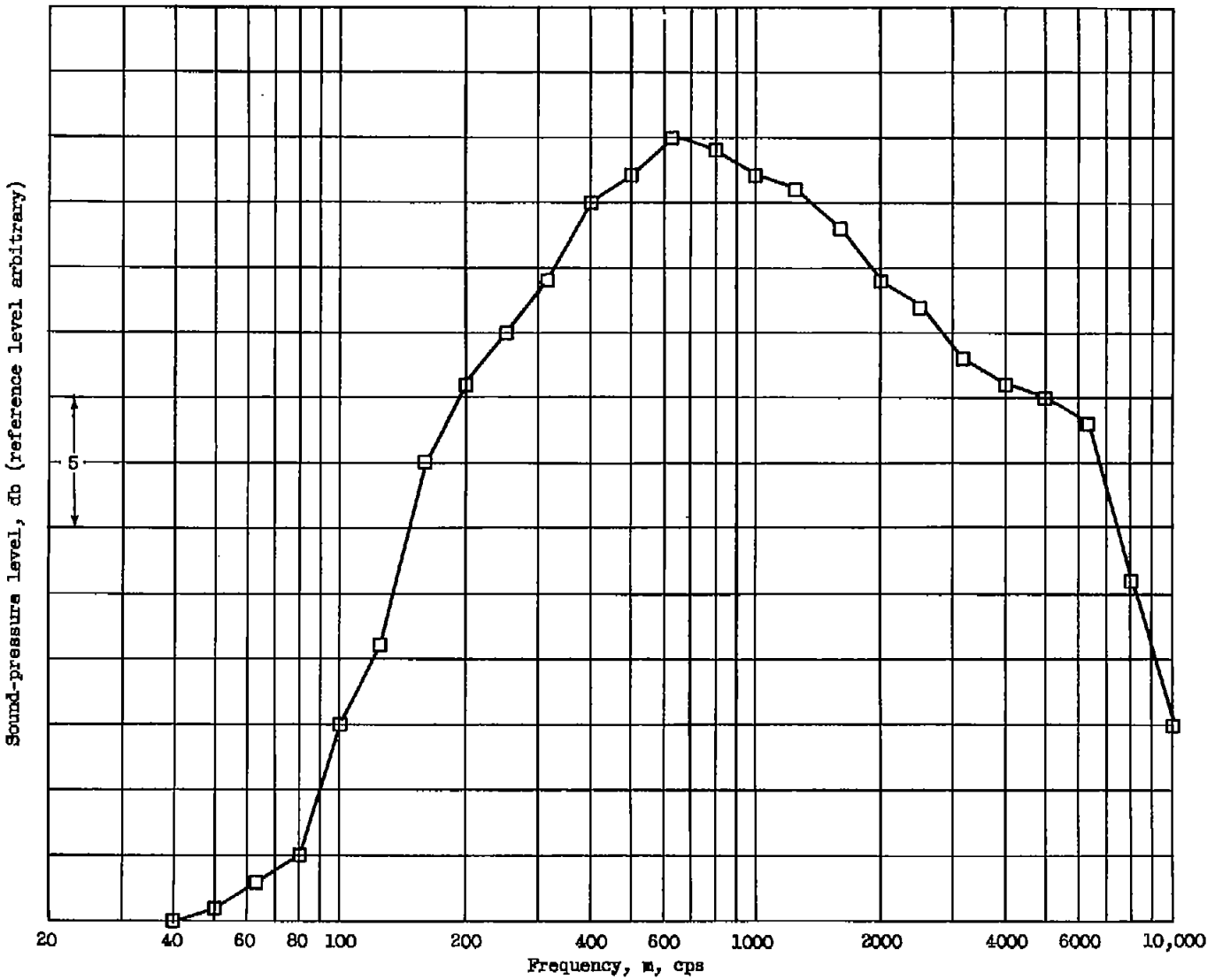

Figure 16. - Sound-pressure-level spectrum at distance of 20 feet from nozzle exit. Run 65; azimuth, 30°; source and receiver heights, 10 feet.

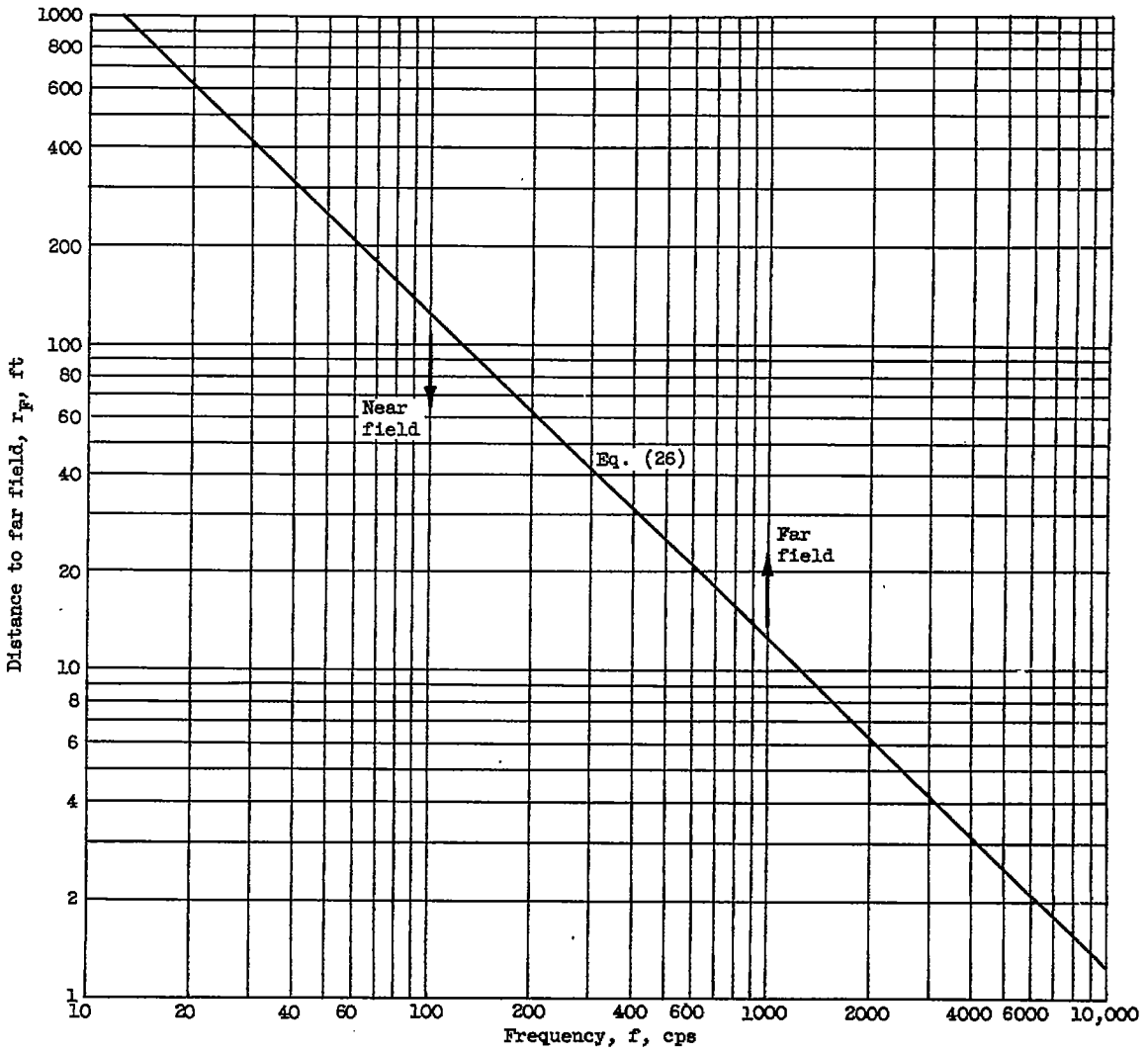

Figure 17. - Distance from jet nozzle exit to onset of far field as function of frequency. Azimuth, 30° or 330°.

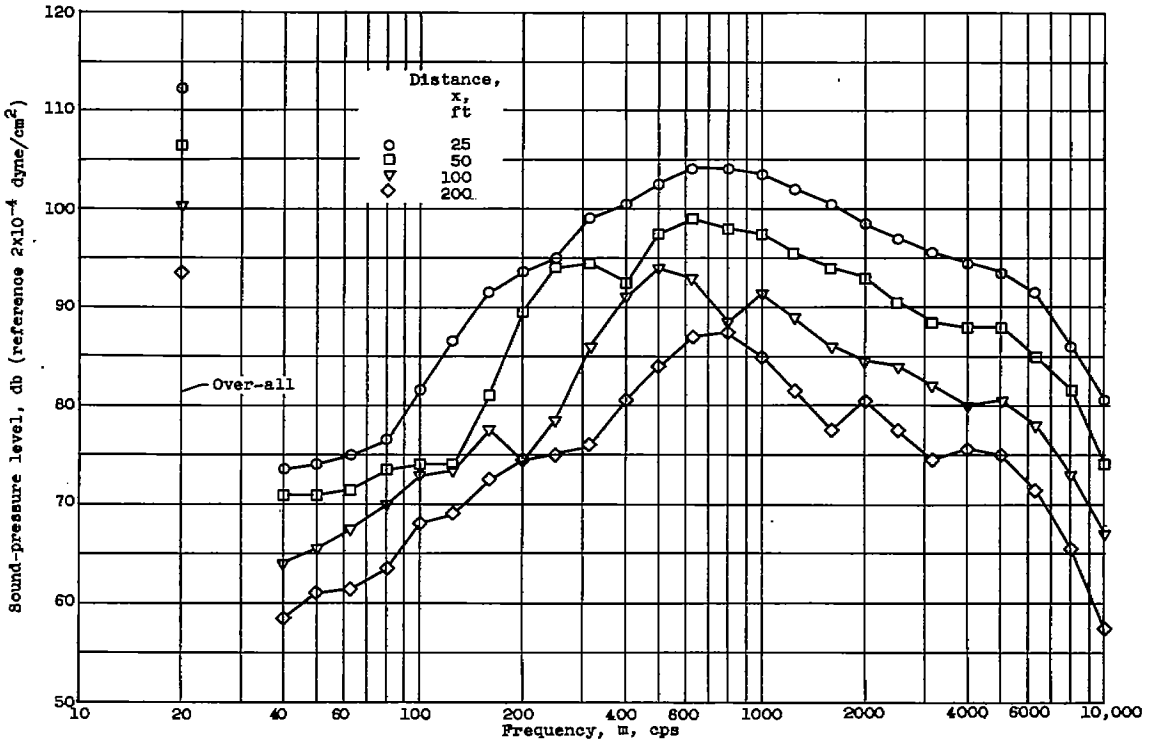

Figure 18. - Experimentally determined sound-pressure-level spectra at various distances from source. Source and receiver heights, 10 feet.

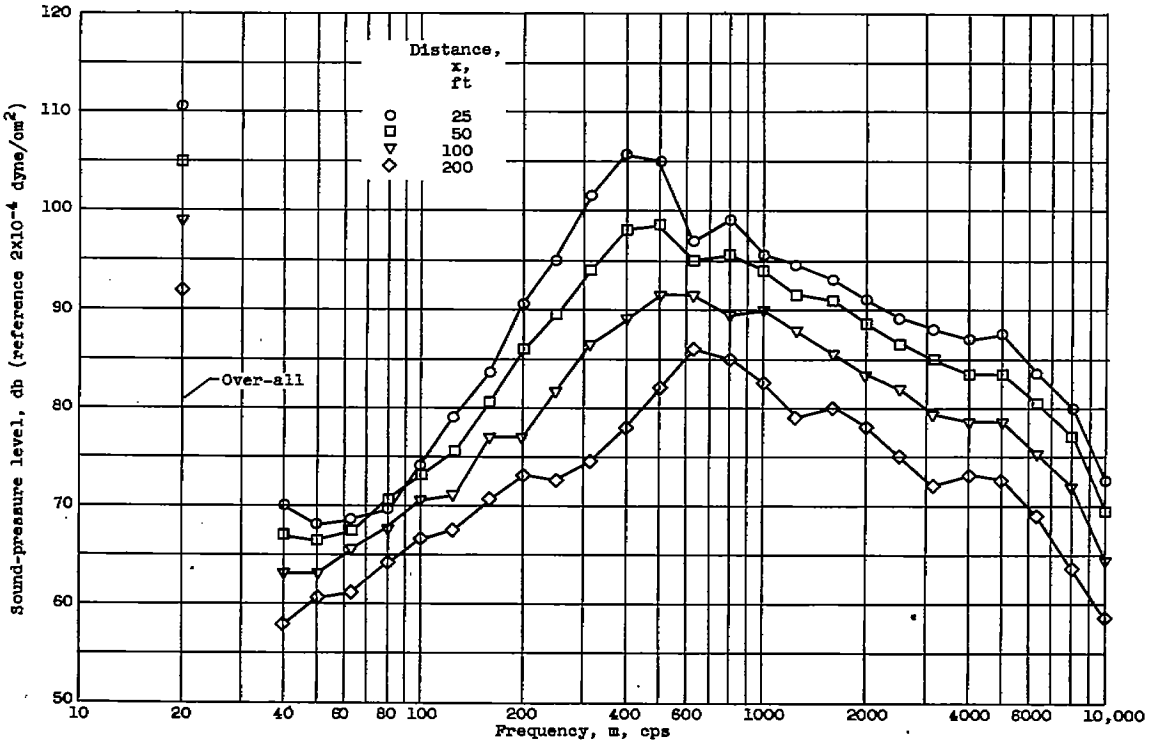

Figure 19. - Corrected sound-pressure-level spectra at various distances from source. Source and receiver heights, 10 feet.

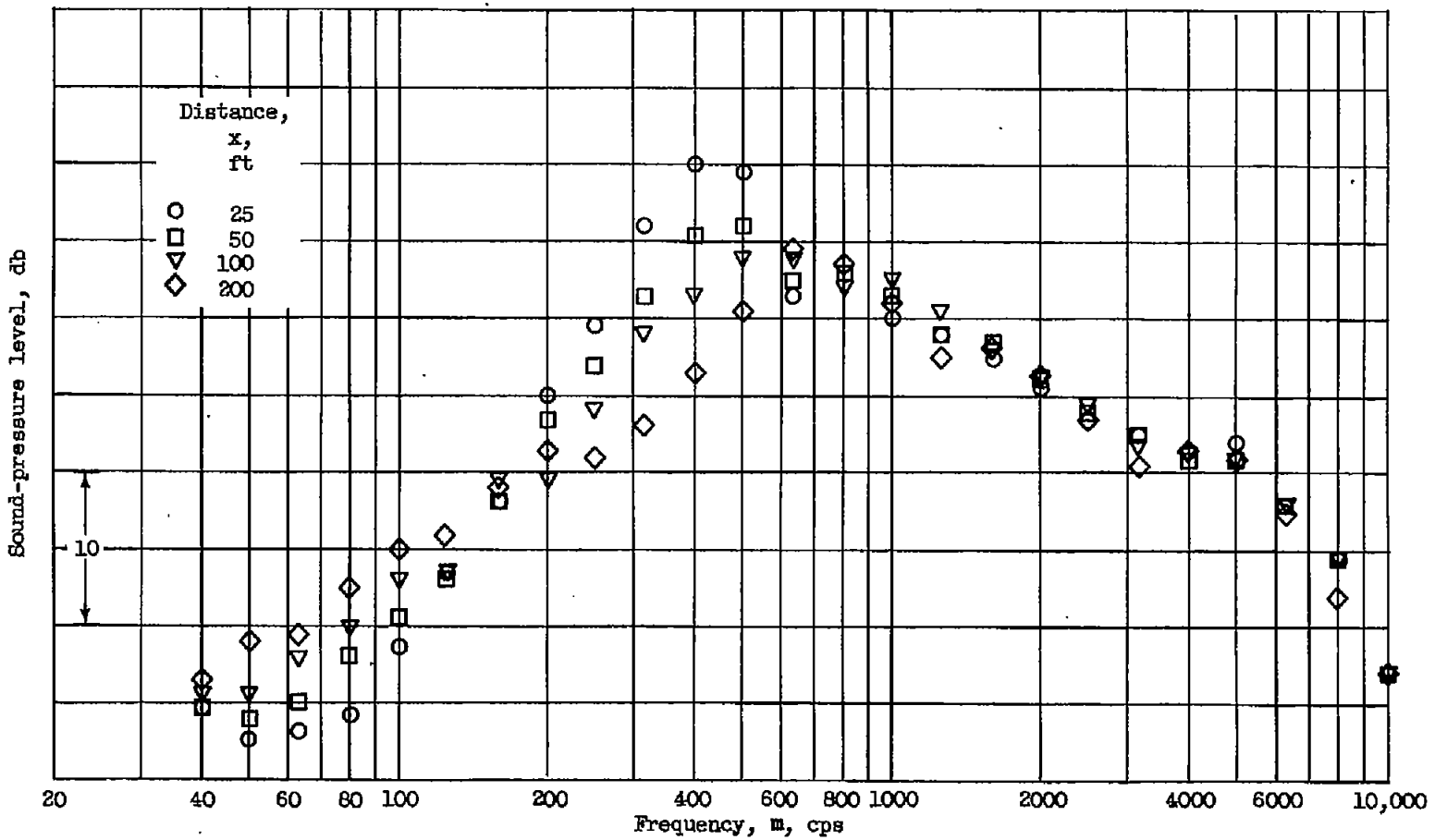

Figure 20. - Comparison of shapes of corrected spectra in figure 19.